Tau pathology in the dorsal raphe may be a prodromal indicator of Alzheimer's disease

Samantha Pierson[1], Kimberly L. Fiock[2], Ruixiang Wang[1], Nagalakshmi Balasubramanian[1], Kanza Khan[3], Ryan Betters[2], Gloria Lee[4,5], Marco M. Hefti[2,5], Catherine A. Marcinkiewcz[1,5]

1. Department of Neuroscience and Pharmacology, University of Iowa, Iowa City, IA 52242
2. Department of Pathology, University of Iowa, University of Iowa, Iowa City, IA 52242
3. Department of Psychological Sciences, Daemen University, Amherst, NY 14226
4. Department of Internal Medicine, University of Iowa, University of Iowa, Iowa City, IA 52242
5. Iowa Neuroscience Institute, University of Iowa, Iowa City, IA 52242

Please address all correspondence to:

Catherine A. Marcinkiewcz

Department of Neuroscience and Pharmacology

2-430 Bowen Science Building

University of Iowa, IA 52242

Email: catherine-marcinkiewcz@uiowa.edu

ABSTRACT

Protein aggregation in brainstem nuclei is thought to occur in the early stages of Alzheimer's disease (AD), but its specific role in driving prodromal symptoms and disease progression is largely unknown. The dorsal raphe nucleus (DRN) contains a large population of serotonin (5-hydroxytryptamine; 5-HT) neurons that regulate mood, reward-related behavior, and sleep, all of which are disrupted in AD. We report here that tau pathology is present in the DRN of cognitively intact individuals 54-80 years of age, whereas synuclein and TDP-43 are relatively absent. Almost all AD cases had tau pathology in the DRN, whereas only a subset contained TDP-43 or synuclein, but not both. Mice overexpressing human P301L-tau in the DRN also exhibited depressive-like behaviors and hyperactivity without any deficits in spatial memory. There was a negative correlation between the density of Tph2-expressing neurons and phospho-tau (ptau) optical density in P301L-tau^{DRN} mice, although mean Tph2 expression did not differ significantly from the controls. 5-HT neurons were hyperexcitable in P301L-tau^{DRN} mice, and there was an increase in the amplitude of excitatory post-synaptic currents (EPSCs) which is suggestive of increased glutamatergic transmission. Astrocytic density was also elevated in the DRN and accompanied by an increase in GFAP expression, as well as changes in *Htr2a*, *Htr2c* and *Htr3a* gene expression. Additionally, tau pathology was detected in axonal processes in the thalamus, hypothalamus, amygdala, and caudate putamen, suggesting that tau may spread in an anterograde manner to regions outside the DRN. Together, these results suggest that tau pathology accumulates in the DRN in a subset of individuals over 50 years and may lead to prodromal AD symptoms, 5-HT neuronal dysfunction, and activation of local astrocytes. The presence of tau pathology in the DRN combined with psychiatric assessments for depression may be a useful screening tool for individuals at risk for AD.

Key words: Dorsal raphe; serotonin; tau; Alzheimer's; brainstem; astrocytes

Introduction

Alzheimer's disease (AD) is an age-related neurodegenerative disease marked by memory loss and cognitive decline[60]. Neuropathological changes in the brain occur prior to any notable deficits in memory and cognition, making clinical diagnosis during the early stages of AD a significant challenge. There is no cure for AD, but identification of biomarkers of prodromal AD is a high priority for research that may enable earlier diagnosis and intervention to improve quality of life and prevent mortality. Neuropsychiatric symptoms (NPS), such as depression and anxiety, have been reported in the early stages of AD and may be a useful indicator of underlying neuropathology and imminent cognitive decline[19, 41, 47, 63, 70]. While the neural circuits underlying NPS are currently unknown, several lines of evidence suggest that the dorsal raphe nucleus (DRN) may be critically involved. The DRN is a brainstem nucleus with extensive efferent serotonergic projections to the forebrain that have been shown to regulate mood, anxiety, and reward-related behavior [40, 44, 53, 57, 68]. Neurofibrillary tangles (NFTs) in the DRN are present in the post-mortem AD brain and accompanied by marked loss of serotonin (5-hydroxytryptamine; 5-HT) neurons, serotonin transporter (SERT) binding sites, and 5-HT_{1A} receptor binding sites [14, 32, 64]. Grinberg and colleagues in 2009 showed that tau pathology appears in the DRN prior to the entorhinal cortex at Braak Stage 0[21], providing some of the first evidence of a role for DRN tauopathy in the prodromal stages of AD.

The presence of NFTs in the DRN at an early stage of AD seems evident, yet it remains relatively underreported in the literature. Additionally, the timing of its appearance and prevalence in the general population is unknown. Another outstanding question is whether the presence of tau pathology in the DRN can alter cognitive function or induce behavioral symptoms associated with prodromal AD. In the present study, we examined post-mortem DRN sections from a group of individuals aged 54-80 years with no documented history of neurological disease, as well as confirmed AD cases for tau, synuclein and TDP-43 pathology.

We then overexpressed a mutant form of tau (P301L-tau) in the DRN of C57BL/6J mice to determine the impact of tau pathology on behavior, 5-HT neuronal function, neuroinflammation, and the spread of tau pathology to interconnected brain regions. Together, these studies provide the first direct evidence that tau pathology in the DRN can induce depressive-like symptoms, serotonergic dysfunction, and astrocytic activation in the absence of any overt memory impairment. The prevalence of tau pathology in the DRN of cognitively intact individuals suggests that it may be a precursor to AD, especially since almost all AD cases contained tau in this region. Furthermore, tau pathology that is initially confined to the DRN may to spread to other brain regions, leading to the emergence of new symptoms.

Materials and methods

Animals

Male and female C57BL/6J mice (Jackson Labs Stock 000664) were housed in University of Iowa animal facilities, under a 12-hour light-dark cycle with standard lighting and *ad libitum* access to food and water. Estrus cycle stages of female mice were tracked following every behavioral assay, using the method described by Byers et al. [12]. All procedures involving animals were in accordance with the University of Iowa's Institutional Animal Care and Use Committee.

Stereotaxic surgery

All surgeries were performed under aseptic conditions. At 8 weeks of age, mice were deeply anesthetized with 3% (v/v) isoflurane in oxygen and placed in a Kopf Angle 2 stereotax on a heating pad. Isoflurane was maintained at 1.5-2% thereafter. An adeno-associated viral vector (AAV) expressing the human transgene for P301L-tau or green fluorescent protein (GFP) was microinjected into the dorsal raphe nucleus (ML: 0.0; AP: 4.65; DV: -3.3 from Bregma at a 23.58º angle from the ML plane) using a 1 µL Hamilton syringe at 100nL/min (500 nL total). Post-

operative analgesia consisted of two meloxicam injections (0.4 mg/kg, sc or ip) given 24 hours apart.

Viral constructs

The original plasmid used to construct the P301L-tau virus was a generous gift from Gloria Lee. Construction of the AAV (AAV2/8-CBA-P301Ltau-WPRE) was performed by the Viral Vector Core Facility at the University of Iowa. AAV2/8-CAG-GFP-WPRE was also obtained at the Iowa Viral Vector Core.

Reverse transcriptase quantitative PCR (RT-qPCR)

A separate cohort of C57BL/6L mice was injected with AAV expressing P301L-tau or GFP. Four weeks post injection, the mice were decapitated under isoflurane anesthesia and the brains were extracted and immediately flash frozen on dry ice. Micro-punches of the DRN were taken, and total RNA was isolated using TRIzol reagent (Ambion Life Technologies) as described previously [4]. DNA contamination was removed from the RNA using DNA-free DNA removal Kit (Life Technologies). RNA purity and concentration were checked using a Nanodrop 1000 spectrophotometer (Thermo Fisher Scientific). Extracted RNA was reverse transcribed using the iScript cDNA Synthesis Kit (BioRad Laboratories) with the following thermal profile: 25°C for 5 minutes, 45°C for 20 minutes, and 95°C for 1 minute. SYBR green qPCR master mix (BioRad Laboratories) and specific primers for the target genes (Table 1) were used for RT-qPCR. The following thermal profile was used on a CFX96 Real-time-PCR System (BioRad Laboratories): 10 minutes at 95°C; 40 cycles of 30 seconds at 95°C, 30 seconds at 60°C; and then followed with a melt curve analysis profile (60°C to 95°C in 0.5°C increments at a rate of 5 seconds/step). Fold changes in mRNA levels were determined by normalizing to β-actin Ct values using the $2^{-\Delta\Delta CT}$ method [58]. Results are shown as fold change in mRNA levels ± SEM.

Behavior Assays

All behavioral assays took place at least 4 weeks post-surgery and were performed in the following order (in males): Elevated Plus Maze, Open field, Social interaction, Sucrose Preference, Barnes Maze, Forced Swim, Contextual Fear condition. In females, all tests except the Barnes Maze and Forced Swim were performed.

Elevated Plus Maze*:* Mice were placed in the center of an elevated, plus-shaped maze with open and enclosed arms (arms 35cm long, 5cm wide, 60cm off the ground; enclosed arms with 20cm high walls) and allowed to explore for five minutes as reported previously[33]. The assay was performed under dim light (~20 lux in open arms, and < 5 lux in closed arms) with the experimenter blocked from view using an opaque curtain. Sessions were recorded with a Basler GenICam and Media Recorder 4 software (Noldus). Time spent in open and closed arms and distance traveled were analyzed using EthoVision XT15.

Open Field test*:* Mice were placed in the corner of a white 50 x 50 x 25.5cm open box inside of a dimly lit (~ 20 lux), sound attenuated chamber and allowed to explore for 30 minutes[33]. Sessions were recorded with a Euresys piccolo U8H.264 camera mounted at the top of the sound attenuating chamber using Media recorder 4 software. The first 10 minutes of each session were analyzed for the following: time spent in the center of the box and total distance traveled.

Social Interaction test*:* Mice were placed in the center of a three-chambered, clear arena (64x41x21cm) inside of a large, dimly lit (~20 lux) sound-attenuated chamber. Mice acclimated to the arena and could explore all chambers for 10 minutes before a novel conspecific “stranger” mouse was placed under a small metal cage in the left or right chamber. Although the stranger was confined to one chamber under the cage, it was clearly visible to the test animal. An empty cage was placed in the opposite-side chamber [33, 51]. Mice were allowed to roam freely between

all chambers for another 10 minutes and interact with the stranger or empty cage. Video was recorded using Media Recorder 4 software and an Euresys piccolo U8H.264 camera mounted at the top of the sound-attenuated chamber. Behavior was scored by measuring the time mice spent engaged in sniffing, circling, rearing, or otherwise in close proximity to and with their snouts pointed towards the stranger or empty cage.

Sucrose Preference test*:* Mice were placed in PhenoTypers (Noldus) equipped with lickometers and two bottles. One bottle was filled with distilled water and the other with 5% sucrose. The sucrose was kept on the same side each day. The bottoms of the PhenoTypers were lined with the same bedding as the home cages. The number of times the mice licked each bottle was recorded for 5 successive days, in 1-hour long sessions for 4 days, and a 20-minute test session on the 5th day. Lickometer data was acquired by Ethovision XT for each session. The first 10 minutes of this test session was used in the analysis.

Barnes Maze*:* A gray circular maze (91cm diameter, 93cm off the ground) had 20 holes evenly dispersed around the perimeter and was illuminated at ~580 lux. External to the maze were 3 visual cues: a yellow star on the screen that obstructed the experimenter from view, a blue square on the wall adjacent to the maze, and a green triangle on the wall behind the maze. On 3 consecutive days, mice were habituated to the maze and learned the location of a hidden compartment under one of the holes. On all training days, if a mouse did not enter the compartment on its own, it was gently nudged or placed inside by the experimenter. On the first day, mice were placed in the center of the arena with a clear beaker overtop for 30 seconds before being guided to the target and given 3 minutes to enter the chamber under the maze. A white noise was played until the mice entered the chamber and stopped upon entry, and they remained in the chamber for 1 minute. On the second day, each mouse received 3 trials of the following: 15 seconds in the center of the maze covered with an opaque box, followed by 2 minutes to freely

move around the maze and enter the escape chamber. If the mouse did not enter the chamber, the clear beaker was placed overtop, keeping them within the vicinity of the chamber, and they were allowed 3 minutes to enter. Mice spent 1 minute in the chamber. While mice were exploring, a loud sustained 100 dB tone was played and then stopped upon chamber entry to serve as a mildly aversive stimulus to incentivize quick locating of and entry into the chamber. On the third day, mice received two of the previously described trials. Mice were given 1 day for consolidation and a break from training (Day 4). On the test day (Day 5), memory was evaluated. The escape chamber was removed, and animals were allowed to freely explore the arena for 2 minutes. Behavior was recorded by an overhead camera and acquired with Ethovision XT 11.5. The distance traveled, velocity, frequency of target and nontarget visits, and time spent in different quadrants of the maze were analyzed in Ethovision.

Forced Swim: The forced swim assay was used to evaluate depressive-like behaviors following injection of AAV-P301L-tau in the DRN of male mice. A tall, clear cylinder was filled with 24-25ºC tap water (32cm height x 20cm diameter; water height 25cm), and mice were gently placed inside for 6 minutes[33]. Following the test, mice were promptly removed from the cylinders and placed in a fresh, dry cage under a heat lamp for 5 minutes to allow them to warm up and dry off. Behavior was recorded from a side view camera and analyzed in Ethovision XT15. Six-minute videos were divided into two phases: a pretest (first 0-2 minutes), and test phase (next 2-6 minutes). Immobility was defined as the absence of movement (excluding tail flicks) for >1 s. Latency to first immobile bout, frequency of immobile bouts, and duration of bouts was measured in Ethovision.

Contextual Fear Conditioning*:* The fear conditioning assay was performed in sound-attenuated operant conditioning boxes manufactured by Ugo Basile (Model 46003) and recorded using a top-mounted infrared camera. A vanilla scent was added to the conditioning chamber as a contextual

cue. On the conditioning day, mice were placed inside of the operant chamber and received a series of 5, 2-second long, 0.6 mA shocks at random intervals ranging from 1-2 minutes following a 2-minute baseline. Sessions ended 2 minutes after the final shock. Twenty-four hours later, mice were placed back in the same chamber for 10 minutes. Time spent freezing during the first 3, 5 and 10 minutes of this test session was determined by a trained observer blinded to the experimental condition. Freezing was scored at 5 s intervals and was defined by the absence of movement for at least 1 s. The data reported represent the first 3 minutes of the test session.

Electrophysiology

Brain Slice Preparation: Mice were deeply anesthetized with tribromoethanol (250 mg/kg, i.p.) and transcardially perfused with ice-cold, carbogenated modified artificial cerebrospinal fluid (aCSF) containing (in mM): 110 choline-Cl, 2.5 KCl, 7 $MgSO_4$, 0.5 $CaCl_2$, 1.25 NaH_2PO_4, 26.2 $NaHCO_3$, 25 glucose, 11.6 Na-ascorbate, 2 thiourea, and 3.1 Na-pyruvate (pH: 7.3 – 7.4; osmolality: 300 – 310 mOsmol/kg). Brains were quickly extracted and sliced with a vibratome (VT1200S; Leica Biosystems) to obtain coronal sections containing the DRN (thickness: 300 µm). The brain slices were recovered in the carbogenated choline-Cl-based aCSF (maintained at 34 °C) for 30 min. Afterwards, they were transferred to a different carbogen-saturated modified aCSF at room temperature in which they were held for at least 1 hour before recordings. The holding aCSF was made with (in mM): 92 NaCl, 2.5 KCl, 2 $MgSO_4$, 2 $CaCl_2$, 1.25 NaH_2PO_4, 30 $NaHCO_3$, 20 HEPES, 25 glucose, 5 Na-ascorbate, 2 thiourea, and 3 Na-pyruvate (pH: 7.3 – 7.4; 300 – 310 mOsmol/kg).

Ex vivo electrophysiological recordings: Neurons were visualized with a differential interference contrast (DIC) microscopy system (BX51W1; Olympus). Membrane currents were amplified by a Multiclamp 700 B amplifier (Molecular Devices), filtered at 3 kHz, and sampled at 20 kHz with a Digidata 1550B digitizer (Molecular Devices). Data were obtained using the pClamp 11 software

(Molecular Devices). In the recording chamber, slices were continuously perfused (2 ml/min) with standard aCSF containing (in mM): 124 NaCl, 4 KCl, 1.2 $MgSO_4$, 2 $CaCl_2$, 1 NaH_2PO_4, 26 $NaHCO_3$, and 11 glucose (300 – 310 mOsmol/kg), saturated with 95% O_2/5% CO_2 and maintained at 30 ± 1°C.

In current clamp recordings for assessing serotonergic excitability, patch electrodes (3 – 5 MΩ) were filled with a solution made with (in mM): 135 K-gluconate, 5 NaCl, 2 $MgCl_2$, 10 HEPES, 0.6 EGTA, 4 Na_2-ATP, and 0.4 Na_2-GTP (pH: 7.3; ~290 mOsmol/kg). In some experiments, currents were injected into the neurons to hold the membrane potential at -70 mV. Input resistance was computed from the decrease in membrane potential upon hyperpolarizing current injection (-100 pA). Rheobase referred to the minimal current that could evoke an action potential. Evoked action potentials were tallied while injecting positive currents for 250 ms at 21 steps (0 – 200 pA, incremented by 10 pA). Data were reported as action potential frequency (number of spikes per 250 ms current step).

In voltage clamp recordings for examining synaptic transmission onto DRN 5-HT neurons, cesium methanesulfonate-based internal solution was used (in mM: 135 cesium methanesulfonate, 10 KCl, 1 $MgCl_2$, 10 HEPES, 0.2 EGTA, 4 Mg-ATP, 0.3 Na_2-GTP, 20 Na_2-phosphocreatine; pH 7.3, ~290 mOsmol/kg, with 1 mg/ml QX-314). Spontaneous excitatory postsynaptic currents (sEPSCs) were recorded continuously for 2 min while the neuron was voltage-clamped at -55 mV; similarly, in the same neuron, spontaneous inhibitory postsynaptic currents (sIPSCs) were recorded while the membrane potential was maintained at +10 mV.

To record electrically evoked EPSCs (eEPSCs) or IPSCs (eIPSCs), a glass pipette containing aCSF was placed lateral to the recorded neuron (distance: ~50 μm), and eEPSCs were evoked by square pulses (duration: 100 μs; 0.1 Hz) at different stimulating intensities (10, 20, 40, 80,

160, and 320 μA) while the neuron was voltage-clamped at -55 mV. Similarly, eIPSCs were evoked while the neuron was held at +10 mV. Moreover, to assess the probability of presynaptic neurotransmitter release, two stimuli with an inter-stimulus interval of 30 ms were delivered at 0.1 Hz, so eEPSCs and eIPSCs were evoked in pairs. The ratio of amplitudes of the two eEPSCs or two eIPSCs, i.e., paired pulse ratio (PPR = eEPSC2/eEPSC1 or eIPSC2/eIPSC1), was computed based on 10 – 30 consecutive trials. To identify 5-HT neurons *post hoc* by immunofluorescence, biocytin (2 mg/ml; Hello Bio) was added into the internal solution, and only Tph2-positive neurons were used in data analysis.

Histology

Mouse Tissue Preparation: Mice were anesthetized with Avertin (Tribromoethanol; 250 mg/kg, i.p.) and transcardially perfused with 30 ml 0.01 M phosphate buffered saline (PBS) followed by 30 ml 4% paraformaldehyde (PFA). Brains were extracted and post-fixed 24 hours in 4% PFA at 4°C, then transferred to PBS with 0.02% sodium azide. Tissues were paraffin-embedded and sectioned at 5 μm using a Leica rotary microtome at the University of Iowa Comparative Pathology Lab.

Human Tissue

De-identified adult brain tissue was obtained from the University of Iowa NeuroBank or the NIH NeuroBioBank at the University of Maryland, Baltimore, MD. Since all samples were de-identified, this does not constitute human subjects research under the NIH Revised Common Rule. All cases had post-mortem intervals less than 24 hours. Alzheimer's disease and Lewy Body Dementia were defined according to standard criteria [2, 49]. All cases were reviewed by one of the authors (MMH), an experienced neurodegenerative and developmental neuropathologist.

DAB staining

All 3,3′-Diaminobenzidine (DAB) staining for ptau and α-synuclein in sectioned mouse and human tissue was performed by the University of Iowa Comparative Pathology Lab. TDP-43 DAB staining was carried out by the Department of Pathology's Immunohistochemistry Lab. DAKO autostainers (Agilent) were used by both labs, and all DAB-stained tissue was counterstained with hematoxylin after the DAB protocols.

AT8 (phospho-tau Ser202/Thr205): Paraffin-embedded slides were placed in distilled water (dH_20) and transferred to citrate buffer (pH 6.0) at 110°C for 15 minutes and allowed to cool for 20 minutes. After a 2-minute tap water rinse and then a 2-minute dH_20 rinse, slides were quenched with 3% hydrogen peroxide for 8 minutes and then rinsed again in distilled water. Next were 2 x 5-minute washes in 1X Dako Buffer, 20 minutes in Avidin, and 20 minutes in biotin with brief buffer rinses in between. For mouse tissue only, Rodent Block M (Biocare) was added for 20 minutes before 2 x 5-minute 1X Dako buffer washes. Slides were incubated in AT8 primary antibody (Table 2) diluted in Dako Diluent at 1:1000 for 15 minutes at room temperature (@RT) followed by 2 x 5-minute 1X Dako buffer washes, then mouse HRP secondary (EnVision) for 15 minutes. This was followed by 2 x 5-minute 1X Dako buffer washes, then 5 minutes in DAB, 3 rinses in 1X Dako Buffer, and finally a DAB enhancer for 3 minutes before a final wash in dH_20.

TPH2: Paraffin-embedded slides were placed in dH_20 and transferred to citrate buffer (pH 6.0) at 110°C for 15 minutes and allowed to cool 20 minutes. After a 2-minute tap water rinse and then a 2-minute dH_20, slides were washed in 1X Dako Buffer and quenched with 3% hydrogen peroxide for 8 minutes. After a brief dH_20 rinse, slides were washed twice in 1X Dako Buffer for 5 minutes. Next, slides were placed in Avidin and then biotin for 20 minutes each, with brief buffer rinses in between. Background Buster (Innovex Biosciences) was added to slides for 30 minutes, followed by 2x5-minute 1X Dako Buffer washes. Slides were incubated in TPH2 primary antibody (Table 2) diluted in Dako Diluent at 1:300 for 60 minutes @RT. After 2 x 5-minute 1X Dako buffer washes, rabbit HRP secondary (EnVision) was applied for 30 minutes. Following another 2 x 5-

minute 1X Dako buffer wash, slides received DAB for 5 minutes, and then a rinse in 1X Dako buffer before a DAB enhancer was applied for 3 minutes. Slides received a final rinse in dH_2O.

α-synuclein: The staining protocol for α-synuclein paraffin-embedded slides was the same as described for AT8 except for the blocking step. A 10% goat serum in 1X Dako buffer solution was used for 30 minutes of blocking. α-synuclein primary antibody (Table 2) was then diluted in Dako Diluent at 1:500 and applied to the slides for 15 minutes @RT. Rabbit HRP secondary (EnVision) was applied for 15 minutes.

TDP-43: Staining was performed using the same protocol as AT8, with minor modifications. Quenching with peroxide was only 5 minutes. TDP-43 primary antibody (Proteintech) was diluted at 1:3000 and slides were incubated in this solution for 15 minutes @RT. Slides incubated in rabbit HRP secondary (EnVision) for 15 minutes. DAB was applied for 10 minutes.

Immunofluorescent staining

The same staining protocol was used for mouse and human paraffin-embedded IF staining, with slight alterations to primary antibody concentrations, choice of secondary antibodies, and secondary antibody concentrations (see Table 2).

Slides were heated at 50-60°C to adhere tissue to slides and soften the paraffin. Paraffin was removed in two xylene washes. Tissue was then rehydrated starting with 100% ethanol, then 90%, 70% and double distilled/Milli-Q water. Slides were placed in a water bath in polypropylene Coplin jars that contained antigen retrieval solution (0.514 g sodium citrate, 168 µL Tween 20, 200 mL MiliQ water) for 10 minutes. Slides were rinsed with 0.01 M PBS before hydrophobic barriers were drawn around tissue slices. Blocking solution (3% BSA, 0.4% Triton X-100 in PBS) was applied for one hour @RT and then slides were washed with PBS. Primary antibodies were diluted in the blocking solution and allowed to incubate overnight (18-24 hours) at 4°C in a humidified chamber at the following concentrations: AT8 1:1000 (mouse and human); TPH2 1:500 (both mouse and human); Iba1: 1:200; GFAP 1:1000. After three PBS washes, slides were

incubated in secondary antibodies diluted at 1:500, 1:1000, or 1:2000 in blocking solution and protected from light for 1 hour @RT (See Table 2 for full antibody information). Slides were once again washed with PBS and then coverslipped with Vectashield Antifade mounting medium (Vector Labs) and sealed with clear nail polish.

Confocal microscopy

All fluorescent images were taken on an Olympus Fluoview FV3000 confocal microscope using Olympus objective lenses (UPLSAPO10X2, NA 0.4; UPLXAPO20X, NA 0.8). AT8-TPH2 z-stack images for analysis were taken at 10X, 1.5 optical zoom, step size 1.0 µm. AT8-GFAP-Iba1 z-stack images for analysis were taken at 20X, step size 0.5 µm. Human tissue IF z-stack images were taken at 20X, 2X optical zoom, step size 1.0 µm.

Image Processing and Analysis

Preprocessing of images for analysis was performed in ImageJ. All images were adjusted to the same brightness and contrast settings and subjected to consistent bright outlier removal. Image analysis was done in ImageJ (NIH). Optical Density (OD) values were obtained following the standard protocol found on the ImageJ NIH website, with OD of the image background subtracted to generate a “Net OD”. For semi-quantitation of DAB images, images were scored blinded with supervision and assistance from a certified neuropathologist (MMH). Tau pathology was designated as follows: Multiple areas in multiple fields of view (++); Very little pathology localized to single fields of view (+); No pathology (-). See Supplementary Figure 1 for examples of each.

TPH2 immunostaining defined the DRN for analysis of AT8 and TPH2 in mouse tissue, and the injection site (GFP or AT8 immunostaining) defined regions for analyses of immunological markers. Representative images for figures were prepared in Adobe Photoshop with adjustments to image orientation (Straightening), Hue/Saturation, Brightness/Contrast, and Vibrance.

Statistical Analysis: For comparisons between two groups with one independent variable, Student t-tests were used where appropriate; otherwise Mann-Whitney tests or Kolmogorov-Smirnov (K-S) tests were used. ANOVAS were used for all analyses involving two or more independent variables. Statistical significance was defined as *p<0.05. **p<0.01, ***p<0.001, ****p<0.0001. Data are expressed as mean ± SEM unless otherwise specified.

Results

Tau pathology is present in the DRN of a subset of cognitively intact individuals

The presence of NFTs in the DRN of patients with advanced AD has been reported by several studies[14, 25, 74]. To our knowledge, only one study has reported tau pathology in the DRN of individuals at an early stage of AD[21]. Here we examined post-mortem brain samples from a group of 14 cognitively normal individuals with no known neurological disease as well as 10 AD cases. Tissues were sectioned through the brainstem and stained for tryptophan hydroxylase-2 (Tph2) as an anatomical reference for DRN and phospho-tau (ptau) (Ser202/Thr205) (AT8) to identify tau pathology. After eliminating samples without Tph2 immunoreactivity (Tph2-IR), we were left with 7 controls (54-80 years of age; mean age 65.43 ± 4.50 years) and 10 AD cases (59-98 years, mean age 74.80 ± 3.86 years). We observed ptau-IR in the DRN of 57.14% (4/7) of these control cases, suggesting that the DRN may be one of the initial regions to develop tau pathology before an AD diagnosis. Among those individuals with a confirmed AD diagnosis, 90% (9/10) had significant ptau-IR in the DRN (Table 3, Figure 1a-d, i).

Since the DRN can also be affected in Lewy Body Dementia (LBD)[7], Parkinson's disease (PD)[22] and frontotemporal lobar degeneration with TDP-43-immunoreactive pathology FTLD-TDP)[73], we also stained for pS129-α-synuclein, and pS409/410-TDP-43 (Figure 1e-h). Only one control case, which was positive for tau, showed positive staining for α-synuclein in the

DRN and none were TDP-43 positive. Three AD cases were positive for α-synuclein, all of whom had comorbid LBD. Another 3 cases, without α-synuclein pathology, showed positive staining for TDP-43. These data suggest that α-synuclein and TDP-43 pathology may be less prevalent in the DRN than tau. We then averaged the optical density of ptau staining across AT8- and AT8+ groups in the control and AD cases, which is shown in Figure 1j. To directly compare the control and AD groups, we took the average ptau OD for all cases in that group (AT8+ and AT8-) and found a significant increase in the AD group ($U=10$, $p<0.05$), Figure 1k). Loss of Tph2-IR neurons is reported in advanced post-mortem AD cases, so we next asked whether ptau colocalizes with Tph2 neurons in control and AD cases in our sample. Double immunofluorescence staining in DRN sections indicates that ptau does colocalize with a subset of Tph2-IR neurons in control and AD cases, but it is also found in other types of cells (Figure 1l-o).

Overexpression of P301L-tau in the DRN promotes depressive-like behaviors in mice

We next asked whether the presence of tau pathology in the DRN could induce behavioral impairments associated with prodromal AD. An AAV vector expressing the human P301L-tau mutant or GFP (control) was stereotaxically injected into the DRN of male C57BL/6J mice at 8 weeks of age. Behavioral testing was initiated 4 weeks later. We also tested these mice in the Barnes maze and contextual fear recall test to examine deficits in spatial memory. C57BL/6J mice express endogenous mouse tau which does not form tau aggregates without the introduction of human tau, so tau pathology is only expected in the mice injected with P301L-tau in the DRN (Figure 2a-c). We found that P301L-tau^{DRN} injected mice exhibited a robust deficit in social interaction relative to controls ($F_{1,18}=64.97$, $p<0.0001$, stranger x tau interaction). Bonferroni post-tests revealed that the presence of P301L-tau in the DRN significantly reduced time spent with the stranger ($t_{36}=6.49$, $p<0.0001$) and increased time spent with the empty cage ($t_{36}=4.14$, $p<0.001$) (Figure 2d). There was also a reduction in sucrose preference on the test

day (t_{17}=2.92, p<0.01) (Figure 2e-f). Together, these results are suggestive of depressive-like behaviors in these mice. It should be noted that the groups did not differ significantly in immobility time in the forced swim test (t_{18}=1.056, ns), which is a putative measure of depressive-like behavior (Figure 2g). However, the reliance of this test on immobility as a read-out means that depressive-like behaviors in P301L-tau^{DRN} mice may have obscured by their heightened baseline locomotor activity (reported below).

The elevated plus maze (EPM) is behavioral test that is commonly used to assess generalized anxiety-like behaviors in rodents. Here we did not observe significant group differences in time spent in the open arms (Figure 2h), although there was a trend toward an increase (t_{14}=1.85, p=0.085). There was, however, a significant increase in locomotor activity in the EPM (t_{14}=2.56, p<0.05) (Figure 2i). In the open field test, we also observed an increase in locomotor activity in the first 10 minutes ($t_{10.28}$=2.75, p<0.05, Welch's correction) but no change in time spent in the center of the arena (t_{17}=0.51, ns) (Figure 2j-k). Together, these results indicate that P301L-tau in the DRN may increase locomotion without altering anxiety-like behavior.

We next examined spatial memory in the Barnes Maze and found no evidence of deficits in latency to the target hole (t_{16}=0.50, ns) (Figure 2l) or the frequency of target revisits (t_{16}=0.24, ns) (Figure 2m). There was, however, an increase in the frequency of non-target visits (t_{16}=2.37, p<0.05), although the latency to the first non-target hole (t_{16}=0.43, ns) did not change. Similarly, there was no deficit in spatial memory in the contextual fear recall test, with mice spending equal time freezing during the first 3 minutes on the recall day (t_{18}=0.46, ns) (Figure 2n). These results suggest that while these mice display behavioral depression as well as hyperlocomotion, their spatial memory is still intact.

Sex differences have been reported in the severity of AD neuropathology, with women typically having more NFTs, greater cognitive decline, and accelerated disease progression relative to men [5, 24, 30, 38]. The DRN is a sexually dimorphic region that in enriched in both types of estrogen receptors (ERα and Erβ)[66], so we might expect to observe sex differences in behavioral manifestations of DRN neuropathology. We observed a significant reduction in social interaction in female P301L-tau^{DRN} mice relative to controls ($F_{1,28}$=24.79, p<0.0001, stranger x tau interaction). Bonferroni post-tests indicated a significant reduction in time spent with the stranger (t_{56}=5.11, p<0.0001), but not with the empty cage (t_{56}=2,15, ns) (Figure 3a-b). However, unlike the males, there was no change in sucrose preference (t_{28}=0.464, ns) (Figure 3c-d). There were also no differences in anxiety-like behavior in the EPM (t_{28}=0.424, ns) or open field (t_{28}=1.06, ns), nor any change in locomotor activity in either test (EPM: t_{28}=0.450, ns; OF:t_{28}=1.15, ns) (Figure 3e-h). We also tested for spatial memory deficits in the contextual fear recall test and found no differences between the two groups (t_{28}=0.104, ns) (Figure 3i). Contrary to our expectations, these results indicate that female P301L-tau mice have fewer behavioral impairments relative to controls than males. However, it should be noted that the accelerated rate of decline in women with AD may be related to a post-menopausal reduction in estrogen and progesterone[13, 71], so these differences may only become apparently in aged female mice.

Tau pathology colocalizes with 5-HT neurons in the DRN and activates local astrocytes

The presence of P301L-tau in the DRN is expected to produce an increase in phospho-tau staining in regions of viral spread (Figure 4a-d). We first quantified ptau-Ser202/Thr205 (AT8) optical density (OD) across subregions of the DRN (rostral, mid, caudal) and found a significant main effect of tau ($F_{1,36}$=16.61, p<0.001), but no interaction between tau and subregion. Bonferroni post-tests revealed a significant increase in the rostral DRN ($t_{8.4}$=3.54, p<0.05) in P301L-tau mice relative to GFP-injected mice in an anatomically matched area. This increase in

ptau persisted when slices were pooled across subregions ($t_{8.37}$=3.03, p<0.05; Welch's correction) (Figure 4e). The DRN also contains a significant number of 5-HT neurons that are vulnerable to neurodegeneration in AD and may be sensitive to the presence of tau tangles. We next examined Tph2 neuronal density and optical density in regions of interest (ROIs) that contained AT8 staining. Surprisingly, there was no change in the density of Tph2-expressing neurons in any subregion of the DRN of P301L-tau DRN mice ($F_{1,34}$=0.168, ns) or pooled across subregions ($t_{11.37}$=0.060, ns, Welch's correction) (Figure 4f). Tph2 OD was also unchanged in all subregions ($F_{1,34}$=0.815, ns) and when pooled across all subregions (t_{16}=1.06, ns) (Figure 4g). However, we did observe a negative correlation between Tph2 cell density and AT8 OD in AT8+ regions of the DRN in P301L-tau mice (R^2=0.4707, p<0.05) (Figure 4h). The directionality of this correlation suggests that there may be a reduction in Tph2 as tau pathology accelerates in the P301L-tau group. Although P301L-tau expression was not restricted to 5-HT neurons in this study, a significant proportion of Tph2 neurons within ROIs defined by AT8 immunoreactivity were also AT8+ (Rostral: 34.14 ± 5.56 %, Mid: 35.98 ± 8.23 %, Caudal: 26.21 ± 7.06 %) (Figure 4h).

We then examined astrocytic and microglial markers in the DRN in AT8 immunoreactive areas of the DRN (Figure 4i-l). Here we found a significant increase in GFAP+ optical density (t_{15}=2.65, p<0.05) and GFAP+ astrocytic cell density ($t_{11.31}$=2.88, p<0.05; Welch's correction) (Figure 4m-n). On the other hand, Iba-1 optical density (t_{16}=1.11, ns) and Iba-1+ microglial cell density (t_{16}=0.344, ns) did not change. This increase in astrocytic activity may be indicative of neuroinflammation which could have accounted for the hyperlocomotion exhibited by P301L-tau^{DRN} mice in the EPM and open field tests. This is congruent with a previous study in which IL-1β overexpression in the DRN induced hyperlocomotion or "mania-like behavior" in the EPM [27].

Tau pathology increases 5-HT neuronal excitability and glutamatergic transmission

We next asked whether the presence of tau pathology in the DRN altered the intrinsic excitability of 5-HT neurons in the DRN (Figure 5a-b). The action potential threshold, or rheobase, was significantly lower in P301L-tau^{DRN} mice (t_{27}=2.17, p<0.05), which is suggestive of hyperexcitability (Figure 5c-d). The average resting membrane potential (RMP) was also more depolarized (-57.81 ± 1.71 mV for GFP and -52.38 ± 1.67 mV for P301L-tau, t_{27}=2.24, p<0.05), and there was an increase in the input resistance (t_{27}=2.36, p<0.05) which may account for the reduced action potential threshold (Figure 5e-f). We then looked at action potential frequency at 10 pA current steps from 0-200 pA. This revealed a significant increase in current-induced spiking (Tau x current interaction: $F_{20,540}$=2.71, p<0.0001, Main effect of tau: $F_{1,27}$=4.82, p<0.05). Bonferroni *post hoc* tests also revealed a significant increase at 180 pA (t_{567}=3.08, p<0.05), 190 pA (t_{567}=3.08, p<0.05), and 200 pA steps (t_{567}=3.24, p<0.05) (Figure 5g). Next, we repeated the current-step protocol from a starting potential of -70 mV to adjust for variations in RMP. Here we also observed a significant increase in action potential frequency as a function of current (Tau x current interaction: $F_{20,520}$=3.75, p>0.0001; Main effect of tau: $F_{1,26}$=4.90, p<0.05), and Bonferroni *post hoc* tests also indicated an increase at 180 pA (t_{546}=3.21, p<0.05), 190 pA (t_{546}=3.51, p<0.05), and 200 pA (t_{546}=3.22, p<0.05). (Figure 5h).

The DRN contains glutamatergic neurons and also receives glutamatergic inputs from outside the DRN that may take up tau from the extracellular space. All of this could affect excitatory drive in 5-HT neurons. Alternatively, intracellular signaling cascades on the postsynaptic side may be impacted by the presence of tau pathology in 5-HT neurons. To address this question, we recorded evoked excitatory post-synaptic currents (eEPSCs) in 5-HT neurons and found an increase in eEPSC amplitude (Tau x stimulation intensity interaction: $F_{5,100}$=4.46, p<0.01; Main effect of tau: $F_{1,20}$=4.52, p<0.05). *Post hoc* Bonferroni comparisons were significant at 160 pA (t_{120}=2.99, p<0.05) and 320 pA stimulation intensities (t_{120}=4.08, p<0.001) (Figure 5i-j). There is

also a population of GABAergic interneurons that provide inhibitory input onto 5-HT neurons in the DRN, so any change in the function of these neurons could alter synaptic drive as well. However, we did not see group differences in evoked inhibitory postsynaptic current (eIPSC) amplitude (Tau x stimulation intensity interaction: $F_{5,95}$=0.1334, ns; Main effect of tau $F_{1,19}$=0.080, ns) (Figure 5k). We then calculated the paired pulse ratio (PPR) of eEPSCs to determine whether the presence of tau could alter the probability of transmitter release at glutamatergic synapses onto DRN 5-HT neurons, but we did not see any group differences (t_{20}=0.3532, ns). Likewise, there was no change in PPR of eIPSCs (t_{19}=0.6804, ns), suggesting no change in the probability of GABA release (Figure 5l-m).

We next turned our attention to spontaneous EPSC and IPSCs (sEPSCs and sIPSCs respectively), which are the result of action potential-independent neurotransmitter release. As expected, neither sEPSC nor sIPSC frequencies were altered (EPSC freq: t_{22}=0.1294, ns; IPSC freq: t_{22}=0.0832, ns), suggesting no change in presynaptic transmitter release (Figure 5n-o). We did see a trend toward an increase in sEPSC amplitude, which is consistent with our eEPSC results (t_{22}=1.90, p=0.07), but no change in sIPSC amplitude (t_{22}=0.0011, ns) (Figure 5p). We did see a significant rightward shift in the cumulative frequency distribution curve of sEPSC amplitude (Kolmogorov-Smirnov D=0.1454, p<0.0001), suggesting that P301L-tau mice tend to have a higher number of larger amplitudes sEPSCs (Figure 5q). On the other hand, the cumulative frequency distribution of the inter-event interval (IEI) of sEPSCs did not differ between groups (K-S D=0.0708, ns), once again indicating no change in sEPSC frequency in P301L-tau^{DRN} mice (Figure 5r).

RT-qPCR analysis of 5-HT receptors and astrocytic markers in the DRN

Through immunohistochemical analyses, we observed that overexpression of P301L-tau in the DRN increased GFAP+ cell density and optical density. We also examined the mRNA levels of

GFAP and CD68 (a microglial marker) 4 weeks post-injection of AAV-P301L-tau or AAV-GFP into the DRN. The mRNA levels of *Gfap* were increased (t_9=2.985, p<0.05) in the DRN. However, no change in *Cd68* mRNA expression was observed (Figure 6a). Further, we analyzed the differential expression of monoaminergic genes that are involved in serotonin metabolism in the DRN of P301L-tau and GFP mice. We found no change in the serotonin reuptake transporter (*Sert)* or tryptophan hydroxylase 2 (*Tph2)* gene expression in P301L-tau mice compared to GFP controls. There were also no changes in *Th* or *Ido1* (Figure 6b). Similar gene expression levels between tau and control groups further indicates no effect of tau on monoamine metabolism-related gene expression 4 weeks post-injection. However, we noticed an alteration in mRNA expression for 5-HT receptors 5-HT_{2A}, 5-HT_{2C}, and 5-HT_{3A} (Figure 6c). While *Htr2a* and *Htr3a* expression was decreased (*Htr2a:* t_{12}=2.358, p<0.05); *Htr3a:* t_{11}=3.744, p<0.01), *Htr2c* was increased (t_{12}=2.288, p<0.05) in the DRN of P301L-tau mice compared to GFP controls. Moreover, we observed no change in mRNA expression of *Htr1a* and *Htr1b* in the DRN.

Propagation of tau pathology from the DRN to other brain regions

Tau pathology propagates from one neuron to another by a process known as transsynaptic spread. When initially confined to the entorhinal cortex of C57BL/6J mice by stereotaxic injection of a viral vector encoding P301L-tau, tau pathology was reported to spread to the hippocampus and impair hippocampal-dependent LTP[39]. Likewise, tau fibrils injected into the LC of PS19 mice were found to propagate tau pathology to LC projection areas, as well as sources of LC innervation in the brain, including the hypothalamus, amygdala, bed nucleus of the stria terminalis, and frontal cortex [29]. We examined AT8 staining in areas that are known targets of the DRN 5-HT system, as well as regions that develop tau pathology in the early stages of AD in a subset of P301L-tau^{DRN} mice at approximately 2 months post-injection. These areas included the entorhinal cortex (EC), thalamus (Thal), hippocampus (HP), hypothalamus

(HT), amygdala (AMY), and caudate/putamen (CPu) (Figure 7a-f). Our results suggest that tau pathology can spread from DRN to the thalamus, hypothalamus and amygdala. One of the mice also had AT8 staining in the CPu, while none had evidence of tau pathology in the entorhinal cortex or hippocampus (Figure 7g). It should be noted that the tau pathology was mostly confined to axon terminals and was not detected in neuronal perikarya. However, we think it is possible that tau pathology may accumulate in these downstream targets over time and would eventually be taken up by adjacent cell bodies.

Discussion

Alzheimer's disease is a fatally progressive neurodegenerative disease that will affect an estimated 8.4 million Americans by 2030[24]. It is often diagnosed in the later stages when cognitive impairment has already progressed to an advanced stage, with current treatments being ineffective at preventing further decline. Early detection and intervention are imperative to halt the progression of neuropathology before widespread neurodegeneration occurs, but it requires predictive biomarkers and diagnostic criteria that can be implemented in the clinic. The establishment of early biomarkers of AD that proceed neurodegeneration by several years or decades would represent a breakthrough for AD diagnosis and prevention. Our human data strongly suggests that tau pathology in the DRN may be an early biomarker of AD that manifests well in advance of any overt cognitive symptoms. This is supported by several other studies in the literature indicating that subcortical nuclei are affected by tau pathology prior to involvement of the entorhinal cortex[21, 62, 65]. Although we cannot know for certain whether these individuals without cognitive impairment would have gone on to develop dementia, our behavioral data in P301L-tau^{DRN} mice suggests that the presence of tau pathology in the DRN can promote depressive-like behavior which is one of the hallmarks of prodromal AD. These behavioral changes coupled with serotonergic dysfunction, astrocyte activation, and tau propagation to other brain regions are all consistent with an early AD profile.

One of the main limitations of this study is that appropriate sections of the DRN are often not available from banked brains, such that our human data is based on a relatively small number of cases. Despite standardized protocols for brain banking, the small size and cytologic diversity of the DRN means that the level of section is difficult to standardize, precluding accurate assessment of 5-HT neuronal density. However, we were able to assess Tph2 expression and cell density in the mice injected with P301L-tau in the DRN. The finding that Tph2-expressing neurons remained relatively intact in P301L-tau^{DRN} mice was somewhat unexpected, as 5-HT neuronal depletion in AD post-mortem tissue has been reported elsewhere[14]. One possibility that there is some compensatory upregulation of Tph2 in cells with mild to moderate tau accumulation, with Tph2 depletion only occurring in the later stages as tau pathology progresses. This is supported by the fact that there is a negative correlation between Tph2 cell density and AT8 OD in the DRN of P301L-tau^{DRN} mice.

We did observe an increase in the intrinsic excitability and enhanced glutamatergic transmission in these neurons. The increased evoked EPSC amplitude in the absence of any change in PPR suggests a post-synaptic mechanism, which may be due to altered glutamate receptor expression, trafficking, or intracellular signaling. Excessive activity in 5-HT neurons may have accounted for some of the behavioral dysregulation we observed here, including hyperactivity and depressive-like behaviors. In a previous study by Ren and colleagues, different subgroups of 5-HT neurons were shown activate distinct and opposing behavioral programs depending on their downstream projection patterns, and 5-HT neurons that project to subcortical regions tended to promote aversive behaviors[45, 57]. While we did not target specific 5-HT subpopulations in this study, it is possible that hyperactivity in these subcortical projecting 5-HT neurons could underpin the behavioral phenotypes observed here. There is also evidence to suggest that heightened DRN serotonergic activity could underlie some depressive disorders,

with depressed suicide patients exhibiting elevated Tph2 expression in the DRN and its projection areas[3, 9, 23, 35, 55, 67].

Hyperactivity in 5-HT neurons with tau pathology may seem paradoxical, but there is some evidence to suggest that it may be an early indicator of neuronal dysfunction in AD and a precursor to neurodegeneration[11, 52]. The higher protein load puts stress on the cell, so this hyperactivity may be compensatory to maintain network performance in the face of increased energy demands. Once the pathology progresses beyond a certain critical point where the cell can no longer compensate, there may be a subsequent reduction in activity. Another intriguing possibility relates to the fact that there is a marked increase in astrocytic density and GFAP immunoreactivity in P301L-tau^{DRN} mice, which is a well-known hallmark of AD[31]. Astrocytes usually proliferate in response to brain injury or neuroinflammation and can assume a neurotoxic A1 or neuroprotective A2 phenotype[16]. When activated, astrocytes can also modulate neuronal excitability by changing the concentration of K+ ions in the extracellular space, a process known as K+ clearance[6]. Any disruption in these astrocytic K+ clearance mechanisms can result in aberrant neuronal activity, such as the hyperexcitability we have seen in 5-HT neurons. Astrocytes also play a central role in glutamate homeostasis in the CNS, so any perturbations in glutamate uptake or release by local astrocytes could alter the excitatory/inhibitory balance in surrounding neurons and lead to glutamate excitotoxicity[42]. We did observe an increase in sEPSC amplitude in 5-HT neurons, but not frequency, suggesting that synaptic glutamate release is not affected but there may be dysregulation of astrocytic glutamate release or uptake. In cultured hippocampal neurons, it was reported that tau accumulation in astrocytes disrupted Ca^{2+}-dependent gliotransmitter release, which in turn altered glutamate transmission in surrounding neurons[56]. P301L-tau is known to accumulate in both neurons and glia[20], and frontotemporal lobar degeneration (FTLD-tau/P301L) is characterized by the presence of tau-immunoreactive deposits in astrocytic processes [17, 20].

We also observed AT8 immunoreactivity in cells with astrocytic morphology in the DRN of P301L-tau^{DRN} mice in this study (Supplementary Figure 2). This propensity for P301L-tau to accumulate in astrocytes may have altered their K+ buffering, as well as their glutamate uptake capacities, causing a shift toward hyperexcitability in 5-HT neurons.

Astrocytes are also activated in the presence of pro-inflammatory cytokines released by microglia in response to tau pathology, resulting in the neurotoxic reactive A1 phenotype [1, 37, 50, 54]. Although we did not observe a change in microglial density in the DRN, we did see a trend toward an increase in CD68 mRNA expression, which is indicative of activated microglia. A1 astrocytes also upregulate expression of IL-1β, which was previously reported to induce hyperlocomotion in mice when genetically overexpressed in the DRN [16, 27]. This phenotype was also observed in our P301L-tau^{DRN} mice, suggesting that astrocytes may be a key player in the behavioral and neuronal network dysregulation observed here. On the other hand, astrocytes can also be neuroprotective. A study in human subjects with tau pathology indicates that those without dementia contained astrocytes with upregulated glutamate transporter 1 (GLT-1) expression compared to those with dementia, suggesting that GLT-1 may play a neuroprotective role in these astrocytes[34]. In a mouse model of human tau that was under the control of a GFAP promoter, and therefore exclusive to astrocytes, downregulation of GLT-1 preceded tau accumulation[15]. It would be an interesting future direction to quantify GLT-1 expression within astrocytes in P301L-tau^{DRN} mice alongside other neuroprotective markers.

Altered expression of 5-HT receptors in the DRN may also impact network excitability. 5-HT$_{3A}$ receptors are ligand-gated cation channels that rapidly depolarize neurons when bound by 5-HT. It has been suggested that 5-HT$_{3A}$ receptors are expressed in glutamatergic interneurons in the DRN and may stimulate the release of glutamate, which then activates local 5-HT neurons[48]. Overall, 5-HT$_{3A}$ receptor expression was downregulated in the DRN, which may be

a compensatory response to 5-HT hyperexcitability. On the other hand, it was previously reported that 97.5% of GABAergic neurons also express 5-HT_{3A} receptors and are activated in response to stress[36]. While we cannot ascertain the cellular distribution of 5-HT_{3A} mRNA from our bulk RT-qPCR data, this would be an important future direction that may help clarify changes in neuronal excitability and synaptic transmission in tau-injected mice.

We also found that 5-HT_{2A} receptors were downregulated, while 5-HT_{2C} receptors were upregulated in P301L-tau^{DRN} mice. Both 5-HT2 receptor subtypes are expressed in GABAergic neurons and have the potential to suppress GABAergic transmission, so they may in fact cancel each other out[59]. Activation of 5-HT_{2C} receptors in DRN GABAergic neurons has been shown to reduce 5-HT neuronal firing and alleviate anxiety[61], which we did not observe in this study. In another study, desensitization of 5-HT_{2C} receptors were necessary for the antidepressant response to selective serotonin reuptake inhibitors (SSRIs), suggesting that these receptors may restrain the therapeutic action of SSRIs by increasing inhibitory feedback onto 5-HT neurons[28]. While we did observe depressive-like behaviors in our mice, this was accompanied by an increase in 5-HT excitability rather than a suppression of 5-HT activity. Furthermore, we did not see a change in GABAergic transmission in 5-HT neurons. It is possible that the 5-HT_{2C} upregulation was counterbalanced by a reduction in 5-HT_{2A} or 5-HT_{3A} receptor expression, and therefore not a significant driver of the behavioral phenotypes observed here.

Tau propagation via transneuronal spread is well-documented in the literature and can be accelerated by microglial activation and neural activity[26, 43, 72]. There is also emerging evidence that astrocytes can participate in the spread of tau to other astrocytes or even accelerate transneuronal spread[18, 69]. Our results confirm that tau pathology initially confined to the DRN can propagate to the thalamus, hypothalamus, and amygdala and appears to colocalize with axonal processes. And while the amygdala and hypothalamus have both been

implicated in depressive behaviors, the accumulation of tau in these areas was sparse and not likely to be a significant driver. It is also worth noting that we did not observe overt tau pathology in the entorhinal cortex or hippocampus which are typically affected at the early stages of AD in Braak Stage 1. However, these data represent a single time point at 2 months post-injection, so we cannot rule out the possibility that tau pathology would have spread to these regions at a later time.

To our knowledge, this is one of the first reports of tau pathology in the DRN of individuals without dementia or cognitive impairment. The relatively low abundance of synuclein and the absence of TDP-43 in these individuals support the notion that the DRN may be more susceptible to tau aggregation, which is associated with AD and FTLD-tau. Accordingly, nearly all AD subjects had some degree of tau pathology in the DRN. We also demonstrate for the first time that tau pathology in the DRN is associated with depressive-like behaviors, serotonergic dysregulation, and astrocytic reactivity which may be a precursor to neurodegeneration. Finally, tau was shown to propagate from the DRN to other subcortical regions and may act as a hub for the spread of tau pathology throughout the brain, a process that is accelerated by neural activity and astrocytic uptake of tau. Overall, these studies suggest that tau aggregation in the DRN may be an early indicator of AD, especially when combined with late-onset depression. Regular screening for late-onset depression may lead to an earlier diagnosis in individuals at risk for AD and could be used in concert with newer MRI and PET imaging tools that can detect brainstem tau pathology or pathological changes in DRN integrity[8, 10, 46].

Acknowledgements: We thank the Li-Chun (Queena) Li and the Iowa Neurobank core for providing human post-mortem tissues for this study, Mariah Leidinger of the Comparative Pathology Core for providing histology services for human and mouse tissues, and the

personnel of the Department of Pathology's Immunohistochemistry Lab for performing TDP-43 staining.

Declarations

Ethics approval: All procedures on mice in this study were approved by the Institutional Care and Use Committee at the University of Iowa.

Availability of data and materials: All data generated or analyzed during this study are included in this published article and its supplementary information files.

Competing Interests: The authors declare that they have no competing interests.

Funding: This work was supported by the National Institute on Alcohol Abuse and Alcoholism (R01 AA028931), the National Institute on Aging (R01 AG070841), and the Williams-Cannon Fellowship to C.A.M. S.P. was supported by the National Institute of General Medical Sciences (T32 GM067795) and K.K. was supported by the National Institute of Diabetes and Digestive and Kidney Disease (T32 DK112751).

References

1. Aloisi F, Borsellino G, Caré A, Testa U, Gallo P, Russo G, Peschle C, Levi G Cytokine regulation of astrocyte function: in-vitro studies using cells from the human brain. Int J Dev Neurosci 13:265–74. doi: 10.1016/0736-5748(94)00071-a
2. Attems J, Toledo JB, Walker L, Gelpi E, Gentleman S, Halliday G, Hortobagyi T, Jellinger K, Kovacs GG, Lee EB, Love S, McAleese KE, Nelson PT, Neumann M, Parkkinen L, Polvikoski T, Sikorska B, Smith C, Grinberg LT, Thal DR, Trojanowski JQ, McKeith IG (2021) Neuropathological consensus criteria for the evaluation of Lewy pathology in post-mortem brains: a multi-centre study. Acta Neuropathol 141:159–172. doi: 10.1007/s00401-020-02255-2
3. Bach-Mizrachi H, Underwood MD, Tin A, Ellis SP, Mann JJ, Arango V (2008) Elevated expression of tryptophan hydroxylase-2 mRNA at the neuronal level in the dorsal and median raphe nuclei of depressed suicides. Mol Psychiatry 13:507–13, 465. doi: 10.1038/sj.mp.4002143

4. Balasubramanian N, Sagarkar S, Choudhary AG, Kokare DM, Sakharkar AJ (2021) Epigenetic Blockade of Hippocampal SOD2 Via DNMT3b-Mediated DNA Methylation: Implications in Mild Traumatic Brain Injury-Induced Persistent Oxidative Damage. Mol Neurobiol 58:1162–1184. doi: 10.1007/s12035-020-02166-z
5. Barnes LL, Wilson RS, Bienias JL, Schneider JA, Evans DA, Bennett DA (2005) Sex Differences in the Clinical Manifestations of Alzheimer Disease Pathology. Arch Gen Psychiatry 62:685. doi: 10.1001/archpsyc.62.6.685
6. Bellot-Saez A, Kékesi O, Morley JW, Buskila Y (2017) Astrocytic modulation of neuronal excitability through K+ spatial buffering. Neurosci Biobehav Rev 77:87–97. doi: 10.1016/j.neubiorev.2017.03.002
7. Benarroch EE, Schmeichel AM, Sandroni P, Parisi JE, Low PA (2007) Rostral raphe involvement in Lewy body dementia and multiple system atrophy. Acta Neuropathol 114:213–20. doi: 10.1007/s00401-007-0260-3
8. Betts MJ, Kirilina E, Otaduy MCG, Ivanov D, Acosta-Cabronero J, Callaghan MF, Lambert C, Cardenas-Blanco A, Pine K, Passamonti L, Loane C, Keuken MC, Trujillo P, Lüsebrink F, Mattern H, Liu KY, Priovoulos N, Fliessbach K, Dahl MJ, Maaß A, Madelung CF, Meder D, Ehrenberg AJ, Speck O, Weiskopf N, Dolan R, Inglis B, Tosun D, Morawski M, Zucca FA, Siebner HR, Mather M, Uludag K, Heinsen H, Poser BA, Howard R, Zecca L, Rowe JB, Grinberg LT, Jacobs HIL, Düzel E, Hämmerer D (2019) Locus coeruleus imaging as a biomarker for noradrenergic dysfunction in neurodegenerative diseases. Brain 142:2558–2571. doi: 10.1093/brain/awz193
9. Boldrini M, Underwood MD, Mann JJ, Arango V (2005) More tryptophan hydroxylase in the brainstem dorsal raphe nucleus in depressed suicides. Brain Res 1041:19–28. doi: 10.1016/j.brainres.2005.01.083
10. Brendel M, Jaworska A, Probst F, Overhoff F, Korzhova V, Lindner S, Carlsen J, Bartenstein P, Harada R, Kudo Y, Haass C, van Leuven F, Okamura N, Herms J, Rominger A (2016) Small-Animal PET Imaging of Tau Pathology with 18F-THK5117 in 2 Transgenic Mouse Models. J Nucl Med 57:792–8. doi: 10.2967/jnumed.115.163493
11. Busche MA, Konnerth A (2015) Neuronal hyperactivity--A key defect in Alzheimer's disease? Bioessays 37:624–32. doi: 10.1002/bies.201500004
12. Byers SL, Wiles M v., Dunn SL, Taft RA (2012) Mouse estrous cycle identification tool and images. PLoS One 7. doi: 10.1371/journal.pone.0035538
13. Carroll JC, Rosario ER, Chang L, Stanczyk FZ, Oddo S, LaFerla FM, Pike CJ (2007) Progesterone and estrogen regulate Alzheimer-like neuropathology in female 3xTg-AD mice. J Neurosci 27:13357–65. doi: 10.1523/JNEUROSCI.2718-07.2007
14. Chen CP, Eastwood SL, Hope T, McDonald B, Francis PT, Esiri MM (2000) Immunocytochemical study of the dorsal and median raphe nuclei in patients with Alzheimer's disease prospectively assessed for behavioural changes. Neuropathol Appl Neurobiol 26:347–55
15. Dabir D v, Robinson MB, Swanson E, Zhang B, Trojanowski JQ, Lee VM-Y, Forman MS (2006) Impaired glutamate transport in a mouse model of tau pathology in astrocytes. J Neurosci 26:644–54. doi: 10.1523/JNEUROSCI.3861-05.2006

16. Ding Z-B, Song L-J, Wang Q, Kumar G, Yan Y-Q, Ma C-G (2021) Astrocytes: a double-edged sword in neurodegenerative diseases. Neural Regen Res 16:1702–1710. doi: 10.4103/1673-5374.306064
17. Ferrer I, López-González I, Carmona M, Arregui L, Dalfó E, Torrejón-Escribano B, Diehl R, Kovacs GG (2014) Glial and neuronal tau pathology in tauopathies: characterization of disease-specific phenotypes and tau pathology progression. J Neuropathol Exp Neurol 73:81–97. doi: 10.1097/NEN.0000000000000030
18. Fleeman RM, Proctor EA (2021) Astrocytic Propagation of Tau in the Context of Alzheimer's Disease. Front Cell Neurosci 15:645233. doi: 10.3389/fncel.2021.645233
19. Geda YE, Roberts RO, Knopman DS, Petersen RC, Christianson TJH, Pankratz VS, Smith GE, Boeve BF, Ivnik RJ, Tangalos EG, Rocca WA (2008) Prevalence of neuropsychiatric symptoms in mild cognitive impairment and normal cognitive aging: population-based study. Arch Gen Psychiatry 65:1193–8. doi: 10.1001/archpsyc.65.10.1193
20. Goedert M, Crowther RA, Spillantini MG (1998) Tau mutations cause frontotemporal dementias. Neuron 21:955–8. doi: 10.1016/s0896-6273(00)80615-7
21. Grinberg LT, Rüb U, Ferretti REL, Nitrini R, Farfel JM, Polichiso L, Gierga K, Jacob-Filho W, Heinsen H, Brazilian Brain Bank Study Group (2009) The dorsal raphe nucleus shows phospho-tau neurofibrillary changes before the transentorhinal region in Alzheimer's disease. A precocious onset? Neuropathol Appl Neurobiol 35:406–16. doi: 10.1111/j.1365-2990.2009.00997.x
22. Grinberg LT, Rueb U, Alho AT di L, Heinsen H (2010) Brainstem pathology and non-motor symptoms in PD. J Neurol Sci 289:81–8. doi: 10.1016/j.jns.2009.08.021
23. Hale MW, Shekhar A, Lowry CA (2011) Development by environment interactions controlling tryptophan hydroxylase expression. J Chem Neuroanat 41:219–26. doi: 10.1016/j.jchemneu.2011.05.002
24. Hebert LE, Weuve J, Scherr PA, Evans DA (2013) Alzheimer disease in the United States (2010-2050) estimated using the 2010 census. Neurology 80. doi: 10.1212/WNL.0b013e31828726f5
25. Hendricksen M, Thomas AJ, Ferrier IN, Ince P, O'Brien JT (2004) Neuropathological study of the dorsal raphe nuclei in late-life depression and Alzheimer's disease with and without depression. Am J Psychiatry 161:1096–102. doi: 10.1176/appi.ajp.161.6.1096
26. Hopp SC, Lin Y, Oakley D, Roe AD, DeVos SL, Hanlon D, Hyman BT (2018) The role of microglia in processing and spreading of bioactive tau seeds in Alzheimer's disease. J Neuroinflammation 15:269. doi: 10.1186/s12974-018-1309-z
27. Howerton AR, Roland A v, Bale TL (2014) Dorsal raphe neuroinflammation promotes dramatic behavioral stress dysregulation. J Neurosci 34:7113–23. doi: 10.1523/JNEUROSCI.0118-14.2014
28. Io Iacono L, Ielpo D, Parisi C, Napoli G, Accoto A, di Segni M, Babicola L, D'Addario SL, Guzzo SM, Pascucci T, Ventura R, Andolina D (2021) MicroRNA-34a regulates 5-HT2C expression in dorsal raphe and contributes to the anti-depressant-like effect of fluoxetine. Neuropharmacology 190:108559. doi: 10.1016/j.neuropharm.2021.108559
29. Iba M, McBride JD, Guo JL, Zhang B, Trojanowski JQ, Lee VM-Y (2015) Tau pathology spread in PS19 tau transgenic mice following locus coeruleus (LC) injections of synthetic

tau fibrils is determined by the LC's afferent and efferent connections. Acta Neuropathol 130:349–62. doi: 10.1007/s00401-015-1458-4

30. Irvine K, Laws KR, Gale TM, Kondel TK (2012) Greater cognitive deterioration in women than men with Alzheimer's disease: A meta analysis. J Clin Exp Neuropsychol 34:989–998. doi: 10.1080/13803395.2012.712676
31. Kaur D, Sharma V, Deshmukh R (2019) Activation of microglia and astrocytes: a roadway to neuroinflammation and Alzheimer's disease. Inflammopharmacology 27:663–677. doi: 10.1007/s10787-019-00580-x
32. Kepe V, Barrio JR, Huang S-C, Ercoli L, Siddarth P, Shoghi-Jadid K, Cole GM, Satyamurthy N, Cummings JL, Small GW, Phelps ME (2006) Serotonin 1A receptors in the living brain of Alzheimer's disease patients. Proc Natl Acad Sci U S A 103:702–7. doi: 10.1073/pnas.0510237103
33. Khan KM, Bierlein-De La Rosa G, Biggerstaff N, Pushpavathi Selvakumar G, Wang R, Mason S, Dailey ME, Marcinkiewcz CA (2022) Adolescent ethanol drinking promotes hyperalgesia, neuroinflammation and serotonergic deficits in mice that persist into adulthood. Brain Behav Immun. doi: 10.1016/j.bbi.2022.07.160
34. Kobayashi E, Nakano M, Kubota K, Himuro N, Mizoguchi S, Chikenji T, Otani M, Mizue Y, Nagaishi K, Fujimiya M (2018) Activated forms of astrocytes with higher GLT-1 expression are associated with cognitive normal subjects with Alzheimer pathology in human brain. Sci Rep 8:1712. doi: 10.1038/s41598-018-19442-7
35. Kulikova EA, Kulikov A v (2019) Tryptophan hydroxylase 2 as a therapeutic target for psychiatric disorders: focus on animal models. Expert Opin Ther Targets 23:655–667. doi: 10.1080/14728222.2019.1634691
36. Li X, Chen S, Yang H, Li X, So K-F, Wang L (2020) GABAergic Neurons in the Dorsal Raphe Nucleus that Express 5-HT3A Receptors Participate in Responses to Stress Hormones. Neuroscience 441:217–225. doi: 10.1016/j.neuroscience.2020.05.055
37. Liddelow SA, Guttenplan KA, Clarke LE, Bennett FC, Bohlen CJ, Schirmer L, Bennett ML, Münch AE, Chung W-S, Peterson TC, Wilton DK, Frouin A, Napier BA, Panicker N, Kumar M, Buckwalter MS, Rowitch DH, Dawson VL, Dawson TM, Stevens B, Barres BA (2017) Neurotoxic reactive astrocytes are induced by activated microglia. Nature 541:481–487. doi: 10.1038/nature21029
38. Lin KA, Choudhury KR, Rathakrishnan BG, Marks DM, Petrella JR, Doraiswamy PM, Alzheimer's Disease Neuroimaging Initiative (2015) Marked gender differences in progression of mild cognitive impairment over 8 years. Alzheimers Dement (N Y) 1:103–110. doi: 10.1016/j.trci.2015.07.001
39. Liu X, Zeng K, Li M, Wang Q, Liu R, Zhang B, Wang J-Z, Shu X, Wang X (2017) Expression of P301L-hTau in mouse MEC induces hippocampus-dependent memory deficit. Sci Rep 7:3914. doi: 10.1038/s41598-017-04305-4
40. Lowery-Gionta EG, Marcinkiewcz CA, Kash TL (2015) Functional alterations in the dorsal raphe nucleus following acute and chronic ethanol exposure. Neuropsychopharmacology 40:590–600. doi: 10.1038/npp.2014.205
41. Lyketsos CG, Lopez O, Jones B, Fitzpatrick AL, Breitner J, DeKosky S (2002) Prevalence of neuropsychiatric symptoms in dementia and mild cognitive impairment: results from the cardiovascular health study. JAMA 288:1475–83. doi: 10.1001/jama.288.12.1475

42. Mahmoud S, Gharagozloo M, Simard C, Gris D (2019) Astrocytes Maintain Glutamate Homeostasis in the CNS by Controlling the Balance between Glutamate Uptake and Release. Cells 8. doi: 10.3390/cells8020184
43. Maphis N, Xu G, Kokiko-Cochran ON, Jiang S, Cardona A, Ransohoff RM, Lamb BT, Bhaskar K (2015) Reactive microglia drive tau pathology and contribute to the spreading of pathological tau in the brain. Brain 138:1738–1755. doi: 10.1093/brain/awv081
44. Marcinkiewcz CA (2015) Serotonergic Systems in the Pathophysiology of Ethanol Dependence: Relevance to Clinical Alcoholism. ACS Chem Neurosci. doi: 10.1021/cn5003573
45. Marcinkiewcz CA, Mazzone CM, D'Agostino G, Halladay LR, Hardaway JA, Diberto JF, Navarro M, Burnham N, Cristiano C, Dorrier CE, Tipton GJ, Ramakrishnan C, Kozicz T, Deisseroth K, Thiele TE, McElligott ZA, Holmes A, Heisler LK, Kash TL (2016) Serotonin engages an anxiety and fear-promoting circuit in the extended amygdala. Nature. doi: 10.1038/nature19318
46. Maruyama M, Shimada H, Suhara T, Shinotoh H, Ji B, Maeda J, Zhang M-R, Trojanowski JQ, Lee VM-Y, Ono M, Masamoto K, Takano H, Sahara N, Iwata N, Okamura N, Furumoto S, Kudo Y, Chang Q, Saido TC, Takashima A, Lewis J, Jang M-K, Aoki I, Ito H, Higuchi M (2013) Imaging of tau pathology in a tauopathy mouse model and in Alzheimer patients compared to normal controls. Neuron 79:1094–108. doi: 10.1016/j.neuron.2013.07.037
47. Michelsen KA, Prickaerts J, Steinbusch HWM (2008) The dorsal raphe nucleus and serotonin: implications for neuroplasticity linked to major depression and Alzheimer's disease. Prog Brain Res 172:233–64. doi: 10.1016/S0079-6123(08)00912-6
48. Monti JM, Jantos H (2008) Activation of the serotonin 5-HT3 receptor in the dorsal raphe nucleus suppresses REM sleep in the rat. Prog Neuropsychopharmacol Biol Psychiatry 32:940–7. doi: 10.1016/j.pnpbp.2007.12.024
49. Montine TJ, Phelps CH, Beach TG, Bigio EH, Cairns NJ, Dickson DW, Duyckaerts C, Frosch MP, Masliah E, Mirra SS, Nelson PT, Schneider JA, Thal DR, Trojanowski JQ, Vinters H v., Hyman BT (2012) National institute on aging-Alzheimer's association guidelines for the neuropathologic assessment of Alzheimer's disease: A practical approach. Acta Neuropathol 123:1–11. doi: 10.1007/s00401-011-0910-3
50. Morales I, Jiménez JM, Mancilla M, Maccioni RB (2013) Tau oligomers and fibrils induce activation of microglial cells. J Alzheimers Dis 37:849–56. doi: 10.3233/JAD-131843
51. Moy SS, Nadler JJ, Young NB, Nonneman RJ, Segall SK, Andrade GM, Crawley JN, Magnuson TR (2008) Social approach and repetitive behavior in eleven inbred mouse strains. Behavioural Brain Research 191:118–129. doi: 10.1016/j.bbr.2008.03.015
52. Palop JJ, Chin J, Roberson ED, Wang J, Thwin MT, Bien-Ly N, Yoo J, Ho KO, Yu G-Q, Kreitzer A, Finkbeiner S, Noebels JL, Mucke L (2007) Aberrant excitatory neuronal activity and compensatory remodeling of inhibitory hippocampal circuits in mouse models of Alzheimer's disease. Neuron 55:697–711. doi: 10.1016/j.neuron.2007.07.025
53. Paul ED, Lowry C a (2013) Functional topography of serotonergic systems supports the Deakin/Graeff hypothesis of anxiety and affective disorders. J Psychopharmacol 27:1090–106. doi: 10.1177/0269881113490328

54. Perea JR, Ávila J, Bolós M (2018) Dephosphorylated rather than hyperphosphorylated Tau triggers a pro-inflammatory profile in microglia through the p38 MAPK pathway. Exp Neurol 310:14–21. doi: 10.1016/j.expneurol.2018.08.007
55. Perroud N, Neidhart E, Petit B, Vessaz M, Laforge T, Relecom C, la Harpe R, Malafosse A, Guipponi M (2010) Simultaneous analysis of serotonin transporter, tryptophan hydroxylase 1 and 2 gene expression in the ventral prefrontal cortex of suicide victims. Am J Med Genet B Neuropsychiatr Genet 153B:909–18. doi: 10.1002/ajmg.b.31059
56. Piacentini R, Li Puma DD, Mainardi M, Lazzarino G, Tavazzi B, Arancio O, Grassi C (2017) Reduced gliotransmitter release from astrocytes mediates tau-induced synaptic dysfunction in cultured hippocampal neurons. Glia 65:1302–1316. doi: 10.1002/glia.23163
57. Ren J, Friedmann D, Xiong J, Liu CD, Ferguson BR, Weerakkody T, DeLoach KE, Ran C, Pun A, Sun Y, Weissbourd B, Neve RL, Huguenard J, Horowitz MA, Luo L (2018) Anatomically Defined and Functionally Distinct Dorsal Raphe Serotonin Sub-systems. Cell. doi: 10.1016/j.cell.2018.07.043
58. Schmittgen TD, Livak KJ (2008) Analyzing real-time PCR data by the comparative CT method. Nat Protoc 3:1101–1108. doi: 10.1038/nprot.2008.73
59. Serrats J, Mengod G, Cortés R (2005) Expression of serotonin 5-HT2C receptors in GABAergic cells of the anterior raphe nuclei. J Chem Neuroanat 29:83–91. doi: 10.1016/j.jchemneu.2004.03.010
60. Simic G, Stanic G, Mladinov M, Jovanov-Milosevic N, Kostovic I, Hof PR (2009) Does Alzheimer's disease begin in the brainstem? Neuropathol Appl Neurobiol 35:532–54. doi: 10.1111/j.1365-2990.2009.01038.x
61. Spoida K, Masseck O a, Deneris ES, Herlitze S (2014) Gq/5-HT2c receptor signals activate a local GABAergic inhibitory feedback circuit to modulate serotonergic firing and anxiety in mice. Proc Natl Acad Sci U S A 111:6479–84. doi: 10.1073/pnas.1321576111
62. Stratmann K, Heinsen H, Korf H-W, del Turco D, Ghebremedhin E, Seidel K, Bouzrou M, Grinberg LT, Bohl J, Wharton SB, den Dunnen W, Rüb U (2016) Precortical Phase of Alzheimer's Disease (AD)-Related Tau Cytoskeletal Pathology. Brain Pathol 26:371–86. doi: 10.1111/bpa.12289
63. Taragano FE, Allegri RF, Krupitzki H, Sarasola DR, Serrano CM, Loñ L, Lyketsos CG (2009) Mild behavioral impairment and risk of dementia: a prospective cohort study of 358 patients. J Clin Psychiatry 70:584–92. doi: 10.4088/jcp.08m04181
64. Tejani-Butt SM, Yang J, Pawlyk AC (1995) Altered serotonin transporter sites in Alzheimer's disease raphe and hippocampus. Neuroreport 6:1207–10. doi: 10.1097/00001756-199505300-00033
65. Theofilas P, Dunlop S, Heinsen H, Grinberg LT (2015) Turning on the Light Within: Subcortical Nuclei of the Isodentritic Core and their Role in Alzheimer's Disease Pathogenesis. J Alzheimers Dis 46:17–34. doi: 10.3233/JAD-142682
66. Torres Irizarry VC, Feng B, Yang X, Nirali P, Schaul S, Ibrahimi L, Ye H, Luo P, Carrillo-Sáenz L, Lai P, Kota M, Dixit D, Wang C, Lasek AW, He Y, Xu P (2022) Estrogen signaling in the dorsal raphe regulates binge-like drinking in mice. bioRxiv 2022.09.05.506646. doi: 10.1101/2022.09.05.506646

67. Underwood MD, Khaibulina AA, Ellis SP, Moran A, Rice PM, Mann JJ, Arango V (1999) Morphometry of the dorsal raphe nucleus serotonergic neurons in suicide victims. Biol Psychiatry 46:473–83. doi: 10.1016/s0006-3223(99)00043-8
68. Urban DJ, Zhu H, Marcinkiewcz CA, Michaelides M, Oshibuchi H, Rhea D, Aryal DK, Farrell MS, Lowery-Gionta E, Olsen RH, Wetsel WC, Kash TL, Hurd YL, Tecott LH, Roth BL (2015) Elucidation of the Behavioral Program and Neuronal Network Encoded by Dorsal Raphe Serotonergic Neurons. Neuropsychopharmacology. doi: 10.1038/npp.2015.293
69. Vogels T, Murgoci A-N, Hromádka T (2019) Intersection of pathological tau and microglia at the synapse. Acta Neuropathol Commun 7:109. doi: 10.1186/s40478-019-0754-y
70. Wise EA, Rosenberg PB, Lyketsos CG, Leoutsakos J-M (2019) Time course of neuropsychiatric symptoms and cognitive diagnosis in National Alzheimer's Coordinating Centers volunteers. Alzheimers Dement (Amst) 11:333–339. doi: 10.1016/j.dadm.2019.02.006
71. Wood H (2022) Menopause influences tau pathology. Nat Rev Neurol 18:317. doi: 10.1038/s41582-022-00669-y
72. Wu JW, Hussaini SA, Bastille IM, Rodriguez GA, Mrejeru A, Rilett K, Sanders DW, Cook C, Fu H, Boonen RACM, Herman M, Nahmani E, Emrani S, Figueroa YH, Diamond MI, Clelland CL, Wray S, Duff KE (2016) Neuronal activity enhances tau propagation and tau pathology in vivo. Nat Neurosci 19:1085–92. doi: 10.1038/nn.4328
73. Yang Y, Schmitt HP (2001) Frontotemporal dementia: evidence for impairment of ascending serotoninergic but not noradrenergic innervation. Immunocytochemical and quantitative study using a graph method. Acta Neuropathol 101:256–70. doi: 10.1007/s004010000293
74. Zweig RM, Ross CA, Hedreen JC, Steele C, Cardillo JE, Whitehouse PJ, Folstein MF, Price DL (1988) The neuropathology of aminergic nuclei in Alzheimer's disease. Ann Neurol 24:233–42. doi: 10.1002/ana.410240210

Tables

Table 1: RT-qPCR primers

Gene Name	Forward/Reverse (5'-3')	Sequence
β-actin	Forward	CCAGCCTTCCTTCTTGGGTA
	Reverse	GAGGTCTTTACGGATGTCAACG
Sert	Forward	CAAAACGTCTGGCAAGGTGG
	Reverse	ACACCCCTGTCTCCAAGAGT
Tph2	Forward	GACCCAAAGACGACCTGCTT
	Reverse	CTGCGTGTAGGGGTTGAAGT
Th	Forward	TACTTTGTGCGCTTCGAGGT
	Reverse	GGAACCTTGTCCTCTCTGGC
Ido1	Forward	GTATGTGTGGAACCGAGGGG
	Reverse	TCCAGTTTGCCAGGACACAG
Htr1a	Forward	TACTCCACTTTCGGCGCTTT
	Reverse	GGCTGACCATTCAGGCTCTT
Htr1b	Forward	ACCCTTCTTCTGGCGTCAAG
	Reverse	ACCGTGGAGTAGACCGTGT
Htr2a	Forward	ACCGACATGCCTCTCCATTC
	Reverse	TGACCAGTATGTTTCCCGCA
Htr2c	Forward	GTGCCCGTTTTTCATCACCAA
	Reverse	AGGAGGCTTTTTGTCTGGCTT
Htr3a	Forward	CCATCTTCATTGTGCGGCTG
	Reverse	CTTGTTGGCTTGGAAGGTGG
Cd68	Forward	GGGGCTCTTGGGAACTACAC
	Reverse	GTACCGTCACAACCTCCCTG
Gfap	Forward	TGAATCGCTGGAGGAGGAGA
	Reverse	GCCACTGCCTCGTATTGAGT

Table 2: Antibody Information

Stain	Tissue Type	Antibody	Concentration
AT8-TPH2 IF	Mouse	Mouse anti-phosphotau, Thermofisher MN1020	1:1000
		Cy3 donkey anti-mouse Jackson Immunoresearch 715-165-150	1:500
		Rabbit anti-tryptophan hydroxylase Novus NB100-74555	1:500
		Dylight 405 donkey anti-rabbit Jackson Immunoresearch 711-476-152	1:500
AT8-Iba1-GFAP IF	Mouse	Mouse anti-phosphotau, Thermofisher MN1020	1:1000
		Dylight 405 donkey anti-mouse Jackson Immunoresearch 715-475-150	1:2000
		Rabbit anti-Iba1, Abcam ab178846	1:200
		Cy3 donkey anti-rabbit, Jackson Immunoresearch 711-165-152	1:500
		Chicken anti-GFAP, Abcam ab4674	1:1000
		Alexa 647 dinkey anti-chicken Jackson Immunoresearch 703-605-155	1:2000
AT8-TPH2 IF	Human	Mouse anti-phosphotau, Thermofisher MN1020	1:1000
		Alexa Fluor 555 goat anti-mouse, Abcam ab150114	1:1000
		Rabbit anti-tryptophan hydroxylase Novus NB100-74555	1:500
		Alexa Fluor 488 goat anti-rabbit, Abcam ab150077	1:1000
AT8 DAB	Mouse & Human	Mouse anti-phosphotau, Thermofisher MN1020	1:1000
		HRP Mouse, EnVision K4001	NA
TPH2 DAB	Human	Rabbit anti-tryptophan hydroxylase Novus NB100-74555	1:300
		HRP Rabbit, EnVision K4003	NA
α-synuclein DAB	Human	Rabbit anti-Alpha Synuclein (phospho-S129) Abcam ab51253	1:500
		HRP Rabbit, EnVision K4003	NA
TDP-43 DAB	Human	Rabbit anti-Phospho-TDP-43 (Ser409/410) Proteintech 22309-1-AP	1:3000
		HRP Rabbit, EnVision K4003	NA

Table 3: Post-mortem case demographics

Case ID	Age(yr)	Sex	AD	Braak stage	Other ND	Ptau-DRN	α-syn DRN	TDP-43 DRN	Source
1	80	F	No	NA	No	+	+	-	INC
2	73	F	No	NA	No	-	-	-	INC
3	61	M	No	NA	No	+	-	-	INC
4	80	F	No	NA	No	-	-	-	INC
5	54	M	No	NA	No	+	-	-	INC
6	56	M	No	NA	No	-	-	-	NIH
7	54	F	No	NA	No	+	-	-	NIH
8	61	F	Yes		No	+	-	+	INC
9	74	M	Yes		LBD	+	+	-	INC
10	82	M	Yes		LBD	+	+	-	INC
11	73	M	Yes		No	+	-	-	INC
12	75	M	Yes		LBD	+	+	-	INC
13	72	M	Yes		No	+	-	+	INC
14	59	M	Yes		No	-	-	-	INC
15	65	M	Yes		No	+	-	+	INC
16	98	F	Yes		No	+	-	-	INC
17	89	F	Yes		No	+	-	-	INC

ND=Neurological disease
LBD = Lewy Body Disease
INC = Iowa Neurobank Core
NIH = National Institutes of Health

Figure Legends

Fig. 1 Neurodegenerative markers in the DRN of individuals cognitively normal and with Alzheimer's Disease. Human dorsal raphe nucleus (DRN) sections were taken from post-mortem cases of individuals cognitively normal (Control) and diagnosed with AD at the time of death (AD). **a-b** DAB staining for AT8 (ptauSer202/Thr205) in control (a) and AD cases (b). **c-d** DAB staining of serotonergic cell marker Tryptophan hydroxylase 2 (TPH2) in control (c) and AD (d) cases, delineating the anatomical boundaries of the DRN. **e-f** DAB staining for α-syn (pS129-α-synuclein) in control (e) and AD (f) cases. Black arrowhead in f denotes α-syn+ staining, magnified in inset. **g-h** DAB staining for TDP-43 (pS409/410-TDP-43) in control (g) and AD (h). Black arrowhead in h denotes TDP-43+ staining, magnified in inset. Counterstain in a-h is hematoxylin. aq=cerebral aqueduct. mlf=medial longitudinal fasciculus. scale bars = 200 μm for a-d and 100 μm for e-h. For the insets of f-h, scale bar = 20um. **i** number of cases that are negative for (DRN tau-) and positive for (DRN tau+) tau in the DRN of control and AD groups. **j** Mean optical density values in control and AD cases, separated by presence or absence of tau staining. In a single tau- case among the AD group, OD=0 and does not appear on the axes. **k** Mean optical density values in control and AD cases, collapsed across DRN tau- and DRN tau+ cases. **l-m** Immunofluorescent staining of AT8 (red) and TPH2 (cyan) in tau+ control (l) and AD (m) cases taken at 20X magnification. **n-o** Magnified 40X images of l and m. White arrowheads point to colocalization of AT8 and TPH2 fluorescence. Asterisks denote larger regions of colocalization, such as cell bodies, that appear in magnified images l-o. Scale bar in l-m=100 μm, and 50 μm in n-o. Data are represented as mean ± SEM. *p<0.05.

Fig. 2 DRN tau pathology promotes depressive-like behaviors in male mice. The P301L-tau mutation or green fluorescent protein (GFP) was delivered via adeno-associated virus into the DRN of C57BL/6J mice (n=10 per group, 20 total). **a** Schematic of viral infusion site in the

DRN. **b-c** Representative DAB images of viral P301L-tau placement staining in GFP (b) and P301L-tau animals (c). **d** Graph of mean time GFP (gray) and P301L-tau mice (magenta) spent interacting with a stranger mouse and object in the social interaction assay. **e** X-Y plot of percent sucrose preference across all days of the sucrose preference assay. **f** Bar graph of percent sucrose preference on test day for both groups (day 5). **g** Bar graph depicting the percent of time mice spent immobile in the forced swim assay. **h-i** Time spent in the open arms (h) and distance moved (i) in the elevated plus maze (EPM). **j-k** Time mice spent in the center of the arena (j) and distance moved (k) in the open field test (OFT). **l-m** Latency of first visit (l) and number of revisits (m) to target and non-target holes in the Barnes Maze task. **n** Percent time mice spent immobile in contextual fear conditioning task. Data are represented as mean ± SEM. Scale bar= 500 μm in (b) and 200 μm in (c). *p<0.05, **p<0.01, ***p<0.001, ****p<0.0001.

Fig. 3 DRN tau pathology leads to social deficits in female mice. Female C57BL/6J mice received infusion of the same P301L-tau or GFP virus utilized in male mice (n=15 per group, 30 total). **a** Schematic of viral infusion into the DRN of female mice. **b** Time female mice spent interacting with a stranger mouse and object in the social interaction assay. **c** X-Y plot of sucrose preference across all days of the sucrose preference assay. **d** Bar graph of percent sucrose preference on the final day of testing (day 5). **e-f** Bar graphs displaying time spent in the open arms (e) and distance moved (f) in the EPM. **g-h** Bar graphs of the time spent in the center of the arena (g) and distance moved (h) in the OFT. **i** Bar graph showing the percent time spent immobile in the contextual fear conditioning task. Data is represented as mean ± SEM. ***p<0.001.

Fig. 4 Tau pathology colocalizes with serotonergic DRN neurons and induces local neuroinflammation. a-b Representative images of TPH2 (cyan) and AT8 (red) immunofluorescent staining in the DRN of a mouse that received AAV-GFP at 15X and 40X,

respectively. **c-d** Representative images of a mouse that received AAV-P301L-tau, also at 15X and 40X. White arrowheads point to instances of TPH2 and AT8 colocalization. **e** Bar graph of AT8 optical density (OD) of GFP (gray) and P301L-tau (magenta) animals across subregions of the DRN and pooled across subregions (overall). **f** Bar graph of TPH2+ cell density in ROIs that contained AT8+ staining. **g** Graph of TPH2 OD in ROIs that were AT8+. We observed no differences between GFP and P301L-tau mice. **h** *Left:* Simple linear regression between TPH2+ cell density and AT8 OD in P301L-tau animals. *Right:* Bar graph of the percentage of TPH2+ cells that were also AT8+ in ROIs for P301L-tau animals. **i-j** Immunofluorescent staining for astrocytic marker GFAP (blue) and microglial marker Iba1 (red) in GFP (i) and P301L-tau animals (j) at 20X magnification. **k-l** GFAP and Iba1 IF in GFP (k) and P301L-tau mice (l) at 40X magnification. **m** Bar graphs displaying mean OD of GFAP+ and Iba1+ staining in ROIs expressing AT8. **n** Bar graph displaying GFAP+ and Iba1+ cell density in ROIs. Data are represented as mean ± SEM. Scalebar in a and c= 200 μm; b, d, k, and l = 20 μm. i and j =100 μm. aq=cerebral aqueduct. *p<0.05.

Fig. 5 Neuronal excitability and glutamatergic transmission is elevated in P301L-tau^{DRN} mice. a Stereotaxic injection of AAV encoding P301L-tau and GFP into the DRN. **b** Representative confocal image of recorded neuron containing biocytin. *Left:* Tph2 immunoreactivity (magenta) with recorded neuron indicated with a white arrow. *Center:* AT8 immunoreactivity (cyan) with recorded neuron indicated with a white arrow. *Right:* Merged image containing Tph2, AT8, and biocytin (yellow). **c** *Top:* Representative traces of action potential firing during a current ramp protocol used to compute rheobase (x-axis = 200 ms, y-axis = 50 mV). *Bottom:* Representative traces showing action potential firing during a 200 pA current step (x-axis = 50 ms, y-axis = 50 mV). **d-f** Histogram of mean action potential thresholds (rheobase), resting membrane potential (RMP), and input resistance for control and P301L-tau^{DRN} mice. **g-h** Histogram of action potential frequency as a function of current (0-200 pA)

starting at RMP and at -70 mV. **i** *Top:* Representative traces of eEPSCs at a range of stimulation intensities (10 - 320 µA) (x-axis = 10 ms, y-axis = 500 pA). *Bottom:* Representative traces of eIPSCs (x-axis = 10 ms, y-axis = 200 pA). **j-k** Histogram of mean eEPSC amplitude and amplitude as a function of stimulation intensity. **l** Representative traces of PPR for eEPSCs (x-axis = 10 ms, y-axis = 500 pA) and eIPSCs (x-axis = 10 ms, y-axis = 200 pA). **m** Histogram of mean PPR for eEPSCs and eIPSCs. **n** Representative traces of sEPSCs (x-axis = 100 ms, y-axis = 50 pA) and sIPSCs (x-axis = 200 ms, y-axis = 50 pA) in control and P301L-tau^{DRN} mice. **o-p** Histograms of mean frequency and amplitude of sEPSCs and sIPSCs. **q-r** Cumulative frequency distributions of sEPSC and inter-event intervals (IEIs) in GFP and P301L-tau^{DRN} mice. Data are represented as mean ± SEM unless otherwise indicated. Scalebars = 100 µm. *p<0.05, ***p<0.001, ****p<0.0001.

Fig. 6 Serotonin receptors and glial markers are altered following tau overexpression in DRN. Summary bar graphs of RT-qPCR results from mice infused with GFP (gray) or P301L-tau (magenta) in the DRN. Y-axes represent fold change in mRNA expression levels compared to *β-actin* in the DRN, with genes of interest labeled on the X-axis. **a** mRNA levels for neuroinflammatory genes *Cd68* and *Gfap*, **b** Genes associated with monoamine metabolism, including *Sert, Tph2, Th*, and *Ido1.* **c** 5-HT receptors including *Htr1, Htr1b, Htr2a, Htr2c, Htr3a*. Data are represented as mean ± SEM. *p<0.05, **p<0.01, ***p<0.0001.

Fig. 7 Tau pathology propagates from the DRN to other brain regions. In a subset of male mice (n=4), we evaluated brain regions downstream of the DRN known to be involved in affective changes and memory for AT8 staining. **a-f** Representative images of staining in respective regions at 60X objective magnification. Insets in **b, d-f** are enlarged and cropped from larger images to highlight positive staining. Black arrowheads point to AT8+ staining. **g** Table summarizing semi-quantitation of AT8 staining in downstream regions. NA=no sections

available of the region from that brain, (-) indicates no AT8 staining. (+) indicates very little pathology localized to single fields of view within a region. (++) indicates multiple areas in multiple fields of view with AT8 staining in a region. Scale bars=20 μm. EC=entorhinal cortex, Thal = thalamus, HP= hippocampus, HT=hypothalamus, AMY=amygdala, CPu=caudate/putamen

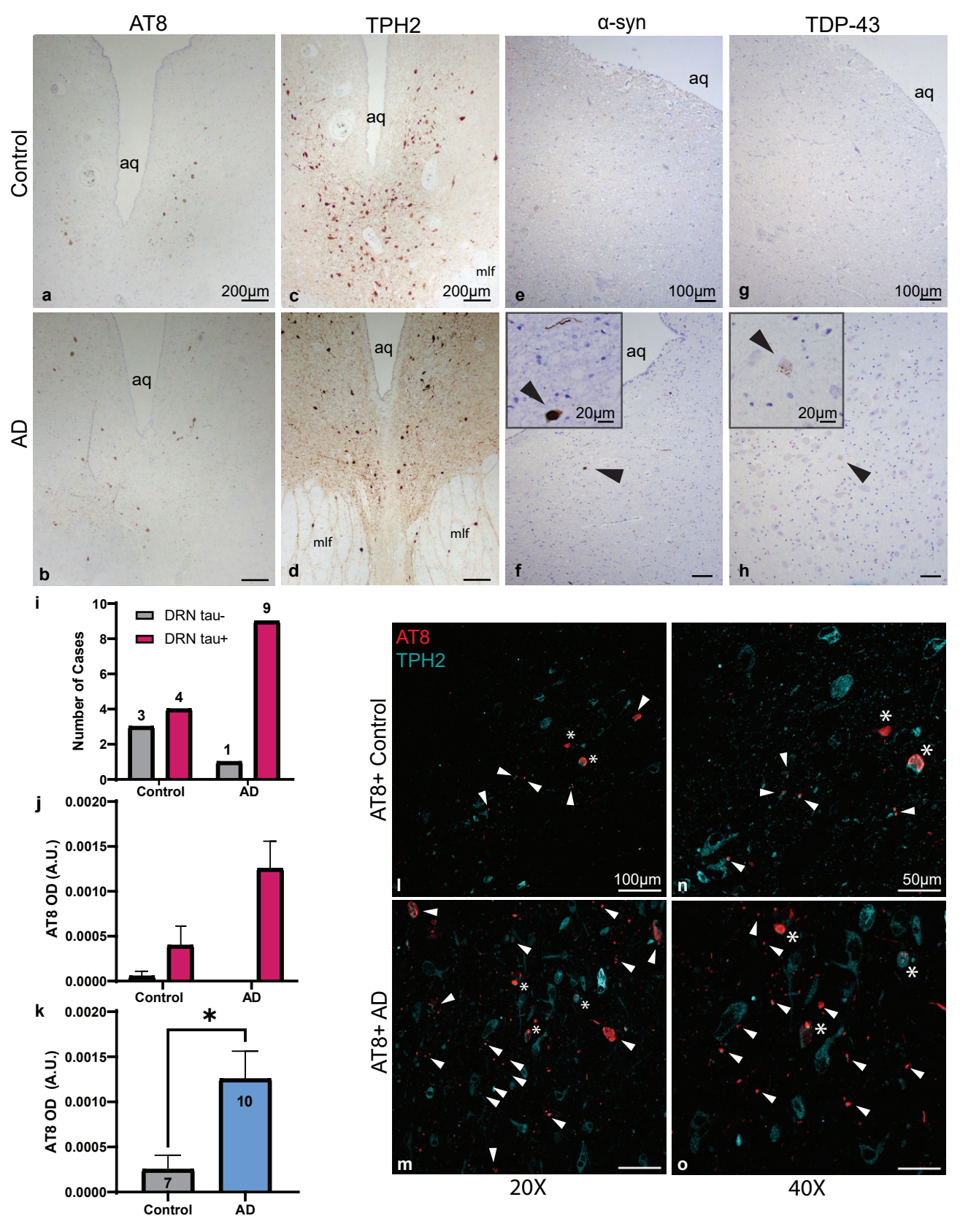
AT8
TPH2
α-syn
TDP-43
Control
AD
aq
mlf
200μm
100μm
20μm
a
b
c
d
e
f
g
h
i
Number of Cases
DRN tau-
DRN tau+
Control
AD
j
AT8 OD (A.U.)
k
AT8+ Control
AT8+ AD
AT8
TPH2
l
m
n
o
50μm
20X
40X

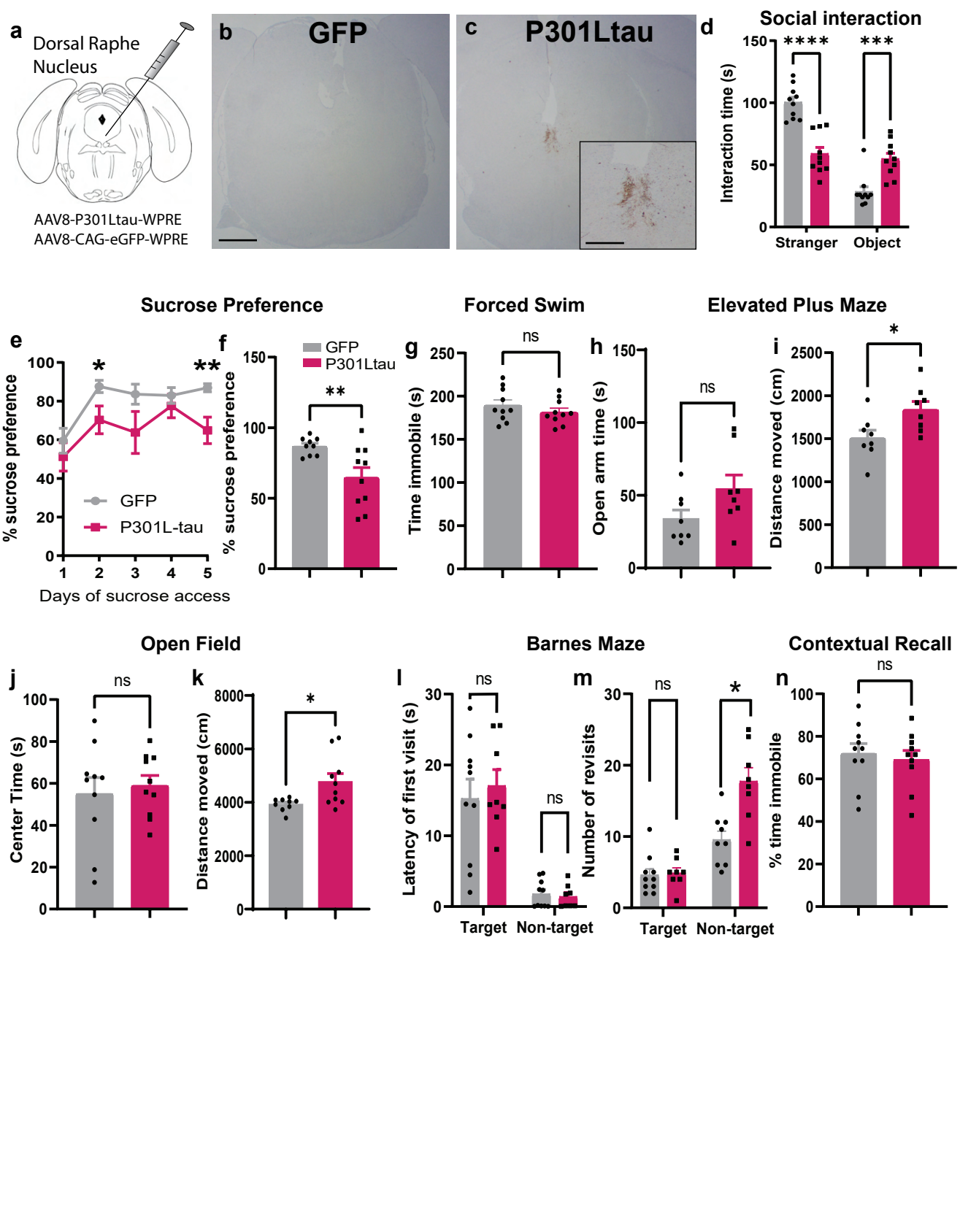
a
Dorsal Raphe Nucleus
AAV8-P301Ltau-WPRE
AAV8-CAG-eGFP-WPRE
b
GFP
c
P301Ltau
d
Social interaction
Interaction time (s)
****
***
Stranger
Object
Sucrose Preference
e
% sucrose preference
GFP
P301L-tau
Days of sucrose access
f
% sucrose preference
GFP
P301Ltau
Forced Swim
g
Time immobile (s)
ns
Elevated Plus Maze
h
Open arm time (s)
ns
i
Distance moved (cm)
Open Field
j
Center Time (s)
ns
k
Distance moved (cm)
Barnes Maze
l
Latency of first visit (s)
Target
Non-target
m
Number of revisits
Target
Non-target
Contextual Recall
n
% time immobile

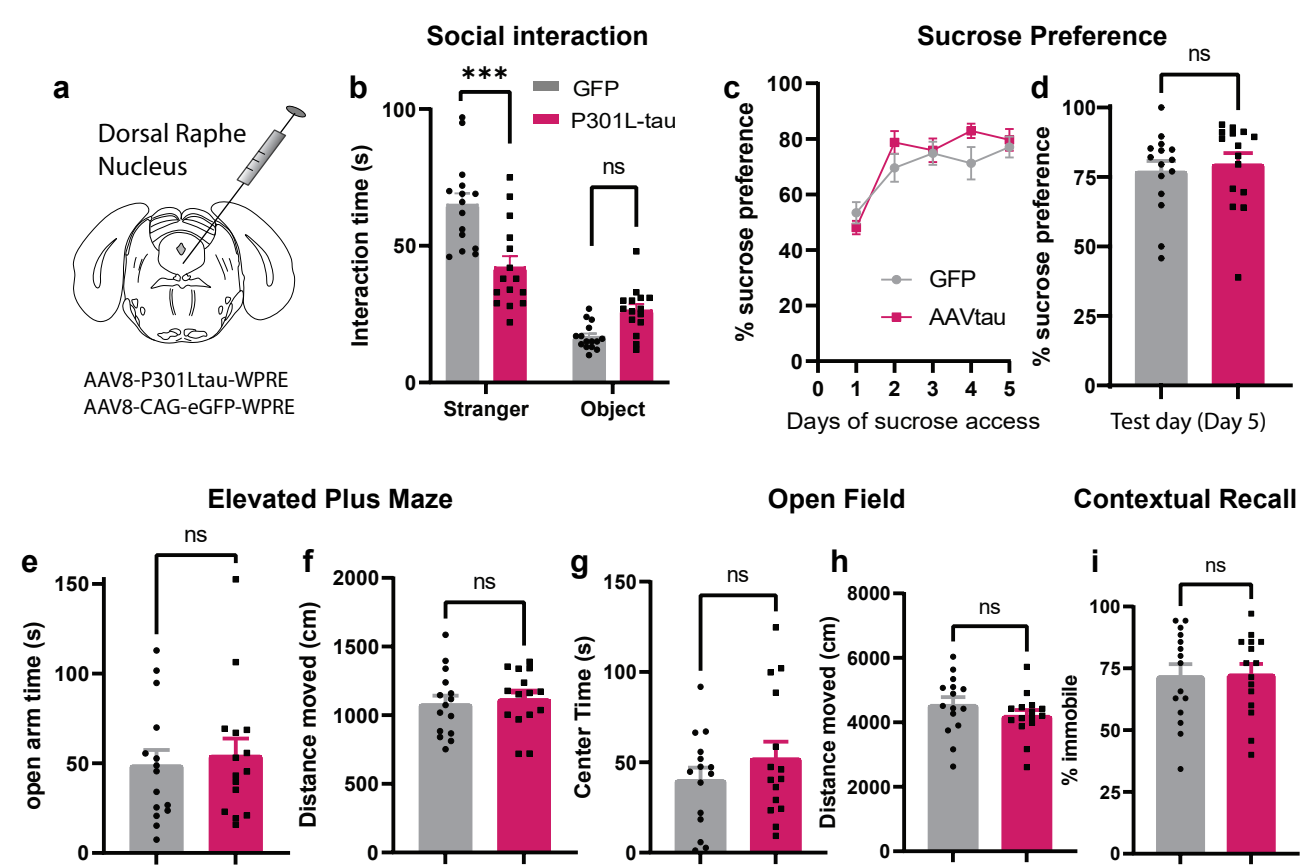
a
Dorsal Raphe Nucleus
AAV8-P301Ltau-WPRE
AAV8-CAG-eGFP-WPRE
Social interaction
b
***
GFP
P301L-tau
ns
Interaction time (s)
100
50
0
Stranger
Object
Sucrose Preference
c
% sucrose preference
100
80
60
40
20
0
GFP
AAVtau
0 1 2 3 4 5
Days of sucrose access
d
ns
% sucrose preference
100
75
50
25
0
Test day (Day 5)
Elevated Plus Maze
e
ns
open arm time (s)
150
100
50
0
f
ns
Distance moved (cm)
2000
1500
1000
500
0
Open Field
g
ns
Center Time (s)
150
100
50
0
h
ns
Distance moved (cm)
8000
6000
4000
2000
0
Contextual Recall
i
ns
% immobile
100
75
50
25
0

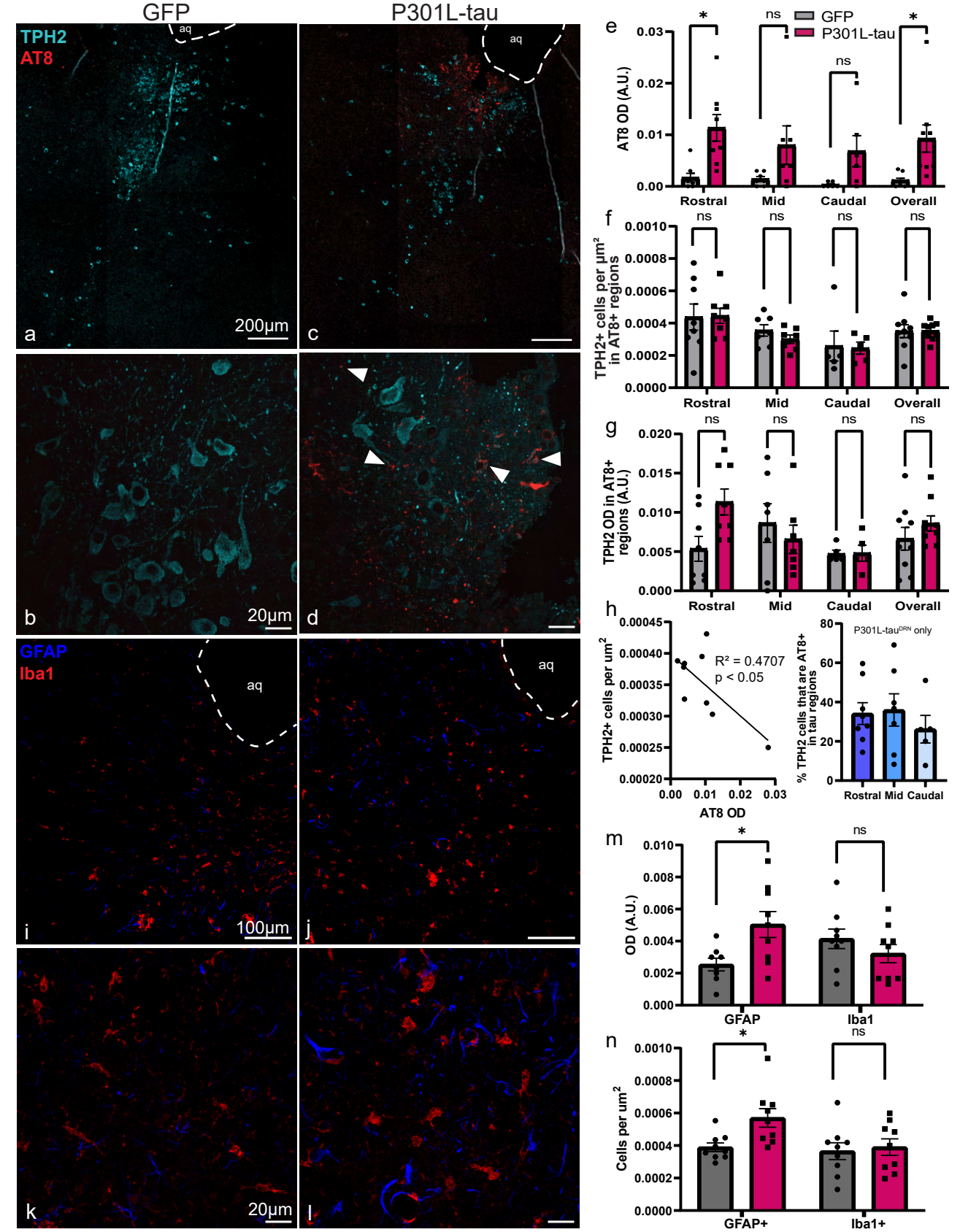
GFP
P301L-tau
TPH2
AT8
aq
200µm
a
c
20µm
b
d
GFAP
Iba1
100µm
i
j
k
l
e
GFP
P301L-tau
AT8 OD (A.U.)
Rostral
Mid
Caudal
Overall
ns
f
TPH2+ cells per µm² in AT8+ regions
g
TPH2 OD in AT8+ regions (A.U.)
h
TPH2+ cells per um²
R² = 0.4707
p < 0.05
AT8 OD
% TPH2 cells that are AT8+ in tau regions
P301L-tauDRN only
m
OD (A.U.)
GFAP
Iba1
n
Cells per um²
GFAP+
Iba1+

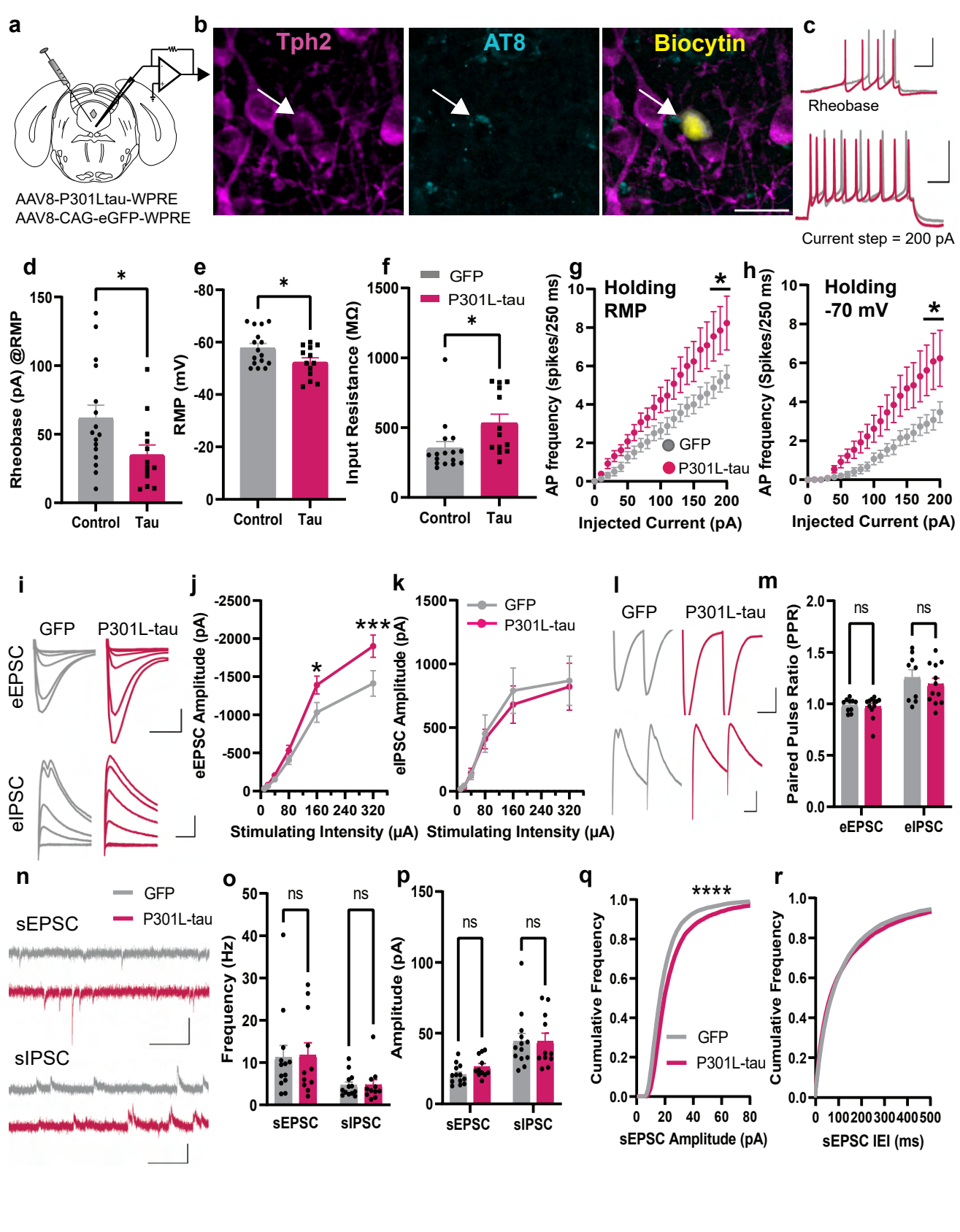
a
AAV8-P301Ltau-WPRE
AAV8-CAG-eGFP-WPRE
b
Tph2
AT8
Biocytin
c
Rheobase
Current step = 200 pA
d
Rheobase (pA) @RMP
Control
Tau
e
RMP (mV)
Control
Tau
f
GFP
P301L-tau
Input Resistance (MΩ)
Control
Tau
g
Holding RMP
AP frequency (spikes/250 ms)
GFP
P301L-tau
Injected Current (pA)
h
Holding -70 mV
AP frequency (Spikes/250 ms)
Injected Current (pA)
i
GFP
P301L-tau
eEPSC
eIPSC
j
eEPSC Amplitude (pA)
Stimulating Intensity (μA)
k
GFP
P301L-tau
eIPSC Amplitude (pA)
Stimulating Intensity (μA)
l
GFP
P301L-tau
m
Paired Pulse Ratio (PPR)
ns
eEPSC
eIPSC
n
GFP
P301L-tau
sEPSC
sIPSC
o
Frequency (Hz)
ns
sEPSC
sIPSC
p
Amplitude (pA)
ns
sEPSC
sIPSC
q
****
Cumulative Frequency
GFP
P301L-tau
sEPSC Amplitude (pA)
r
Cumulative Frequency
sEPSC IEI (ms)

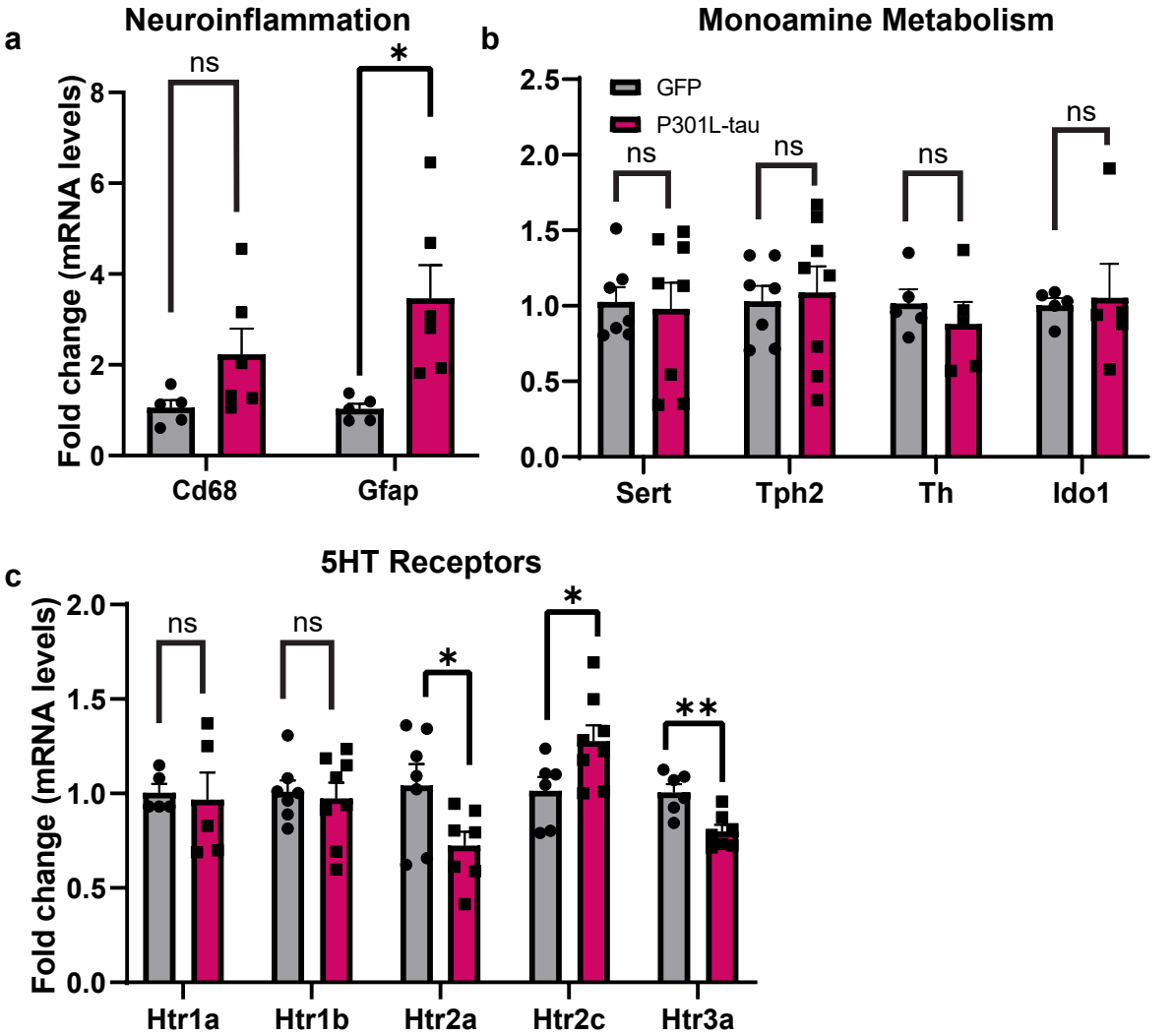
a
Neuroinflammation
Fold change (mRNA levels)
ns
*
Cd68
Gfap
b
Monoamine Metabolism
GFP
P301L-tau
ns
Sert
Tph2
Th
Ido1
c
5HT Receptors
Fold change (mRNA levels)
ns
ns
*
*
**
Htr1a
Htr1b
Htr2a
Htr2c
Htr3a

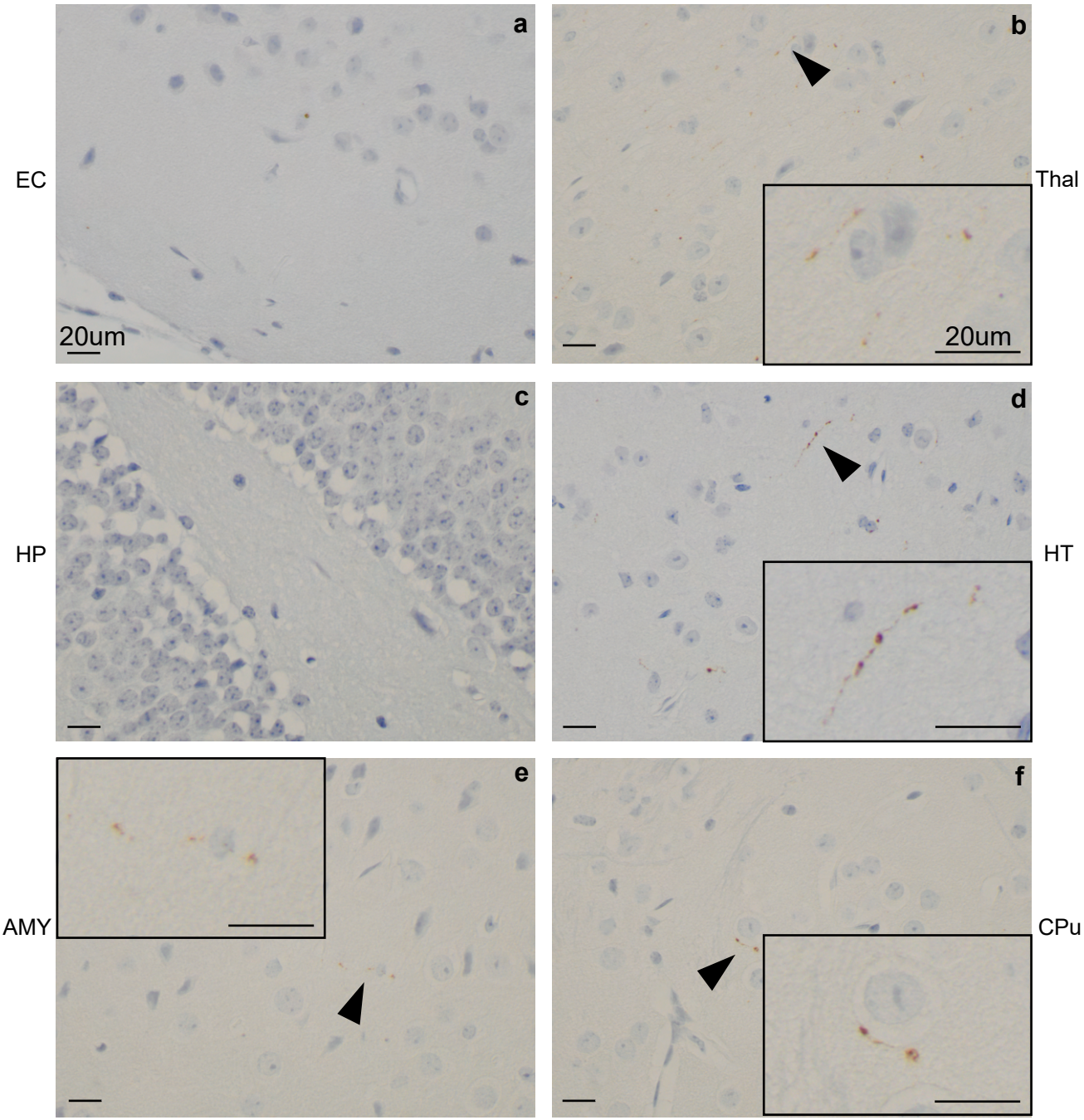

g	EC	HP	Thal	HT	AMY	CPu
Brain1	-	-	++	++	+	+
Brain2	-	-	++	++	+	-
Brain3	-	NA	++	NA	NA	NA
Brain4	-	-	+	+	+	-